Article

Cell

# Adipose Tissue Macrophage-Derived Exosomal miRNAs Can Modulate *In Vivo* and *In Vitro* Insulin Sensitivity

## Graphical Abstract

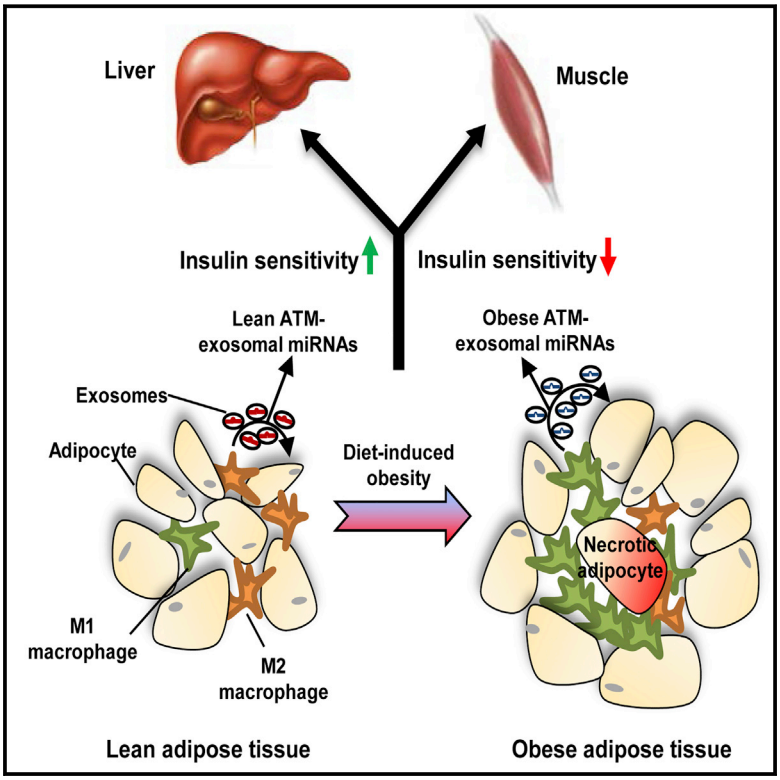


## Highlights

- Exosomes secreted by adipose tissue macrophages transfer miRNAs to insulin target cells
- Treatment of lean mice with obese ATM exosomes causes insulin resistance
- Treatment of obese mice with lean ATM exosomes improves insulin resistance
- Obese ATM exosomes contain miR-155, which can cause insulin resistance

## Authors

Wei Ying, Matthew Riopel, Gautam Bandyopadhyay, ..., Wenxian Fu, Pingping Li, Jerrold M. Olefsky

## Correspondence

jolefsky@ucsd.edu

## In Brief

Macrophages residing in adipose tissue use exosomes to modulate systemic insulin responses.

Ying et al., 2017, Cell *171*, 372–384
October 5, 2017 © 2017 Elsevier Inc.
http://dx.doi.org/10.1016/j.cell.2017.08.035

# Adipose Tissue Macrophage-Derived Exosomal miRNAs Can Modulate *In Vivo* and *In Vitro* Insulin Sensitivity

Wei Ying,[1] Matthew Riopel,[1] Gautam Bandyopadhyay,[1] Yi Dong,[2] Amanda Birmingham,[3] Jong Bae Seo,[1] Jachelle M. Ofrecio,[1] Joshua Wollam,[1] Angelina Hernandez-Carretero,[1] Wenxian Fu,[2] Pingping Li,[4] and Jerrold M. Olefsky[1,5,*]

[1]Division of Endocrinology and Metabolism, Department of Medicine, UC San Diego, 9500 Gilman Drive, La Jolla, CA 92093, USA
[2]Pediatric Diabetes Research Center, Department of Pediatrics, UC San Diego, 9500 Gilman Drive, La Jolla, CA 92093, USA
[3]Center for Computational Biology and Bioinformatics, UC San Diego, 9500 Gilman Drive, La Jolla, CA 92093, USA
[4]State Key Laboratory of Bioactive Substance and Function of Natural Medicines, Institute of Materia Medica, Chinese Academy of Medical Sciences & Peking Union Medical College, Beijing 100050, China
[5]Lead Contact
*Correspondence: jolefsky@ucsd.edu
http://dx.doi.org/10.1016/j.cell.2017.08.035

## SUMMARY

**MiRNAs are regulatory molecules that can be packaged into exosomes and secreted from cells. Here, we show that adipose tissue macrophages (ATMs) in obese mice secrete miRNA-containing exosomes (Exos), which cause glucose intolerance and insulin resistance when administered to lean mice. Conversely, ATM Exos obtained from lean mice improve glucose tolerance and insulin sensitivity when administered to obese recipients. miR-155 is one of the miRNAs overexpressed in obese ATM Exos, and earlier studies have shown that PPARγ is a miR-155 target. Our results show that miR-155KO animals are insulin sensitive and glucose tolerant compared to controls. Furthermore, transplantation of WT bone marrow into miR-155KO mice mitigated this phenotype. Taken together, these studies show that ATMs secrete exosomes containing miRNA cargo. These miRNAs can be transferred to insulin target cell types through mechanisms of paracrine or endocrine regulation with robust effects on cellular insulin action, *in vivo* insulin sensitivity, and overall glucose homeostasis.**

## INTRODUCTION

Insulin resistance is a key component in the etiology of type 2 diabetes mellitus, and obesity is clearly the most common cause of insulin resistance in humans (Johnson and Olefsky, 2013; Kahn et al., 2006; Romeo et al., 2012). As a result of the ongoing global obesity epidemic, there is a parallel rise in the prevalence of type 2 diabetes mellitus (Ogden et al., 2016). One of the hallmarks of obesity in both humans and rodents is a state of chronic, unresolved inflammation in adipose tissue, liver, and possibly skeletal muscle (Hirosumi et al., 2002; Holland et al., 2011; Hotamisligil et al., 1995, 1996; Shoelson et al., 2003; Xu et al., 2003). One of the striking components of this obesity-induced tissue inflammatory response is the accumulation of proinflammatory macrophages, particularly in adipose tissue and liver (Lumeng et al., 2007, 2008; Morinaga et al., 2015; Nguyen et al., 2007; Oh et al., 2012; Weisberg et al., 2003).

A number of earlier studies identified this chronic tissue inflammatory state and suggested that proinflammatory cytokines, such as tumor necrosis factor alpha (TNF-α) are secreted from tissue macrophages and directly inhibit insulin sensitivity, providing a potential cause for obesity-induced insulin resistance (De Taeye et al., 2007; Hotamisligil et al., 1996; Weisberg et al., 2003). However, anti-TNF-α antibody therapies have only led to limited benefits with respect to insulin resistance and glucose metabolism in humans (Dominguez et al., 2005; Lo et al., 2007; Ofei et al., 1996; Paquot et al., 2000), indicating that there must be other macrophage and immune cell factors contributing to decreased insulin sensitivity. Recently, the arachidonic acid-derived eicosanoid leukotriene B4, which works through its specific receptor BLT1 (Toda et al., 2002), has been proposed as one such factor that can directly decrease insulin signaling in hepatocytes and myocytes (Li et al., 2015; Spite et al., 2011). Galectin-3 is another macrophage-secreted factor that can both promote proinflammatory responses and directly block insulin action by inhibiting insulin receptor signaling (Li et al., 2016). In this current paper, we report a new mechanism whereby adipose tissue macrophages (ATMs) can modulate insulin action by secreting microRNA (miRNA) containing exosomes (Exos) into the circulation.

miRNAs are small non-coding RNAs that can serve as regulators of mRNA expression and translational efficiency in most cell types (Bartel, 2004). These miRNAs contain 6- to 8-nucleotide seed sequences, which correspond to complementary sequences in the 3′ UTR of target mRNAs (Brennecke et al., 2005; Lewis et al., 2003, 2005). Binding of the miRNAs to mRNAs leads to recruitment of the target mRNAs to the RNA-induced silencing complex (RISC) leading to translational arrest and mRNA degradation (Ameres et al., 2007; Mallory et al., 2004). Through these mechanisms, miRNAs can decrease protein expression of targeted mRNAs. In addition to their endogenous

 © 2017 Elsevier Inc.

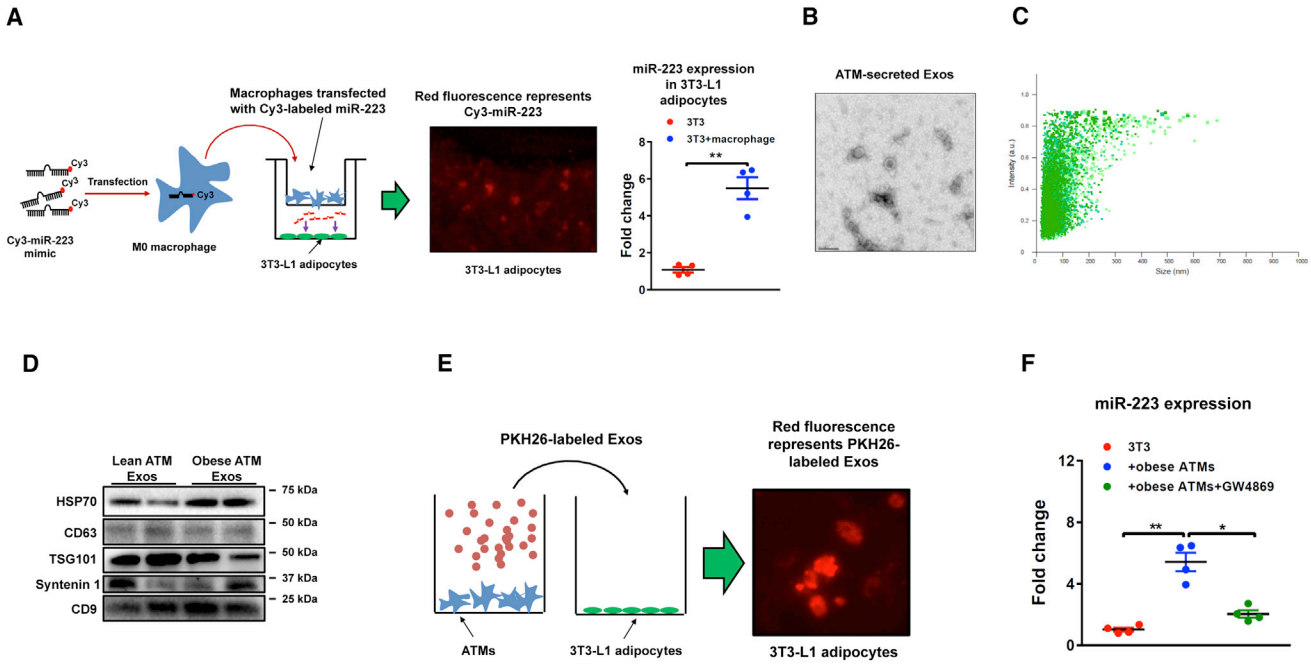


**Figure 1. Macrophages Secrete Exosomal miRNAs**

(A) Naive (M0) macrophages transfected with a Cy3-labeled miR-223 mimic were co-cultured with 3T3-L1 adipocytes in a transwell (membrane pore = 0.4 μm) plate.

(B) Electron microscopy analysis of Exos secreted by obese adipose tissue macrophages (ATMs). Scale bar, 200 nm.

(C) Particle size of the vesicles secreted from obese ATMs was measured by NanoSight analysis.

(D) Exosome (Exo)-specific markers TSG101 and syntenin 1 and extracellular vesicle-related protein markers HSP70, CD63, and CD9 were measured by western blot analysis. These blots are representative of 3 replicated independent experiments, each containing 2 samples.

(E) Exos from obese ATMs were labeled with PKH26 and then added to 3T3-L1 adipocyte cultures.

(F) The effects of the EV secretion inhibitor GW4689 (10 μM) on exosome-dependent miRNA delivery from ATMs into 3T3-L1 recipient cells.

Data are presented as the mean ± SEM. n = 4 per group (A and E); n = 3 (C). *$p < 0.05$, **$p < 0.01$, Student's t test.

See also Figure S1.

actions, miRNAs can be secreted into the extracellular space within nanoparticles termed Exos (Chen et al., 2016; Hulsmans and Holvoet, 2013; Kosaka et al., 2010; Valadi et al., 2007; Zhang et al., 2015a). These cell-derived Exos contain numerous miRNAs, which can work locally or can enter the circulation to act at distal sites. Evidence also exists that these Exos can be taken up into neighboring or distant cell types to modulate the function of recipient cells (Bang et al., 2014; Costa-Silva et al., 2015; Fong et al., 2015; Zhang et al., 2015b). This led us to hypothesize that ATMs secrete exosomal miRNAs, which serve as extracellular molecules that can regulate cellular insulin action and systemic insulin sensitivity.

Here, we report that ATMs from obese animals secrete Exos containing miRNAs that can be taken up into insulin target cells, both *in vitro* and *in vivo*, leading to cellular and systemic insulin resistance and glucose intolerance. In contrast, treatment of obese recipients with ATM-Exos derived from lean mice leads to a robust improvement in glucose tolerance and insulin sensitivity, both *in vivo* and *in vitro*. Finally, we demonstrate that miR-155 is among the differentially expressed miRNAs in obese ATM-Exos and that miR-155 can inhibit insulin signaling and glucose tolerance through a mechanism most likely related to direct suppression of its target gene PPARγ.

## RESULTS

### ATMs Secrete Exosomal miRNAs

We first determined whether macrophages can secrete extracellular miRNAs that are then transported into target cells. MiR-223 is a myeloid cell-selective miRNA (Johnnidis et al., 2008). After transfection of a fluorescent Cy3-labeled miR-223 mimic, bone-marrow-derived macrophages (BMDMs) were co-cultured with 3T3-L1 adipocytes in a transwell plate (Figure 1A). The appearance of red fluorescent Cy3 dye in the 3T3-L1 adipocytes demonstrates that the Cy3-miR-223 mimic was delivered from the BMDMs in the upper transwell to the recipient adipocytes seeded in the lower well (Figure 1A). The Cy3 dye appearance was concomitant with a 6-fold increase in miR-223 abundance in the 3T3-L1 adipocytes after co-culture (Figure 1A). In control experiments, we treated BMDMs with Cy3 alone (not conjugated to miR-223) and found negligible appearance of this fluorescent dye in the BMDMs and no appearance of dye in 3T3-L1 adipocytes after 12 hr co-culture with these BMDMs (Figure S1A). Thus, macrophages can secrete extracellular miRNAs, which are taken up into adipocytes.

Exos are miRNA-containing extracellular vesicles (EVs), which are secreted from cells, and it is known that circulating Exos are a

major mechanism for miRNA transport. To examine whether ATMs can secrete Exos, we isolated ATMs (CD11b+F4/80+) from visceral adipose tissue (VAT) of obese wild-type (WT) mice and then cultured these cells for 72 hr. After removal of dead cells and debris from the conditional medium, electron microscopy (Figure 1B) and NanoSight analysis (Figure 1C) revealed that particles isolated by ultracentrifugation contain abundant ATM-derived EVs with a diameter of 30–100 nm. Density gradient ultracentrifugation analysis (Kowal et al., 2016) of these EVs confirmed that they primarily consist of Exos, as evidenced by expression of the exosome-specific protein markers TSG101, syntenin1, CD63, and miR-155, largely in fractions 3 and 4 (Figures S1B–S1F). Expression of other EV/exosome-associated protein markers CD9 and HSP70 was detected in these fractions (Figure S1C). In addition, Kowal et al. (2016) have reported that the endoplasmic reticulum protein marker Grp94 is excluded from Exos, and this protein was non-detectable in the ATM-derived Exos (Figure S1G). There were no differences in the abundance of any of these exosome-associated protein markers or overall exosome production from lean compared to obese ATMs (Figures 1D and S1H). We also confirmed that the macrophage-derived Exos harbor miRNAs, as evidenced by the robust Cy3 red florescence detected in the Exos secreted by BMDMs transfected with Cy3-miR-223 (Figure S1I).

Next, we tested whether these ATM-Exos can be taken up by adipocytes. These ATM-derived Exos were labeled with the fluorescent dye PKH26 and then added into the culture medium of 3T3-L1 adipocytes. After 12 hr, the 3T3-L1 adipocytes exhibited efficient uptake of the ATM-secreted Exos, as indicated by the presence of red fluorescence staining in these cells (Figure 1E). Furthermore, after co-culture of obese ATMs with 3T3-L1 adipocytes, a several fold increase in ATM-derived miR-223 expression was observed in the adipocytes. Importantly, prior addition (24 hr) of the EV secretion inhibitor GW4869 to the ATMs blocked exosome production and delivery of miR-223 from ATMs into 3T3-L1 adipocytes, showing that macrophages secrete extracellular miRNAs predominantly in an exosome-dependent manner (Figures 1F and S1H). Overall, our results show that macrophages can secrete miRNA-containing Exos, which are then efficiently transported into recipient cells.

## ATM-Derived miRNA-Containing Exos from Obese Mice Promote Insulin Resistance

ATMs in lean tissue primarily display an anti-inflammatory phenotype, whereas obesity increases the number of ATMs and drives them toward a proinflammatory activation state. Substantial evidence indicates that ATMs can mediate inflammation and insulin resistance in obesity. Therefore, we tested whether ATMs can modulate insulin sensitivity *in vivo* by secretion of Exos miRNAs. Insulin-sensitive normal chow diet (NCD)-fed WT lean mice were used as recipients and were intravenously injected with PKH26-labeled ATM-Exos (30 μg every 7 days) derived from obese animals (obese ATM-Exos). The appearance of red fluorescent PKH26 dye in the liver, adipose tissue, and muscle of recipient mice indicates *in vivo* uptake of Exos in these tissues (Figure S2A). All recipient mice exhibited similar body weight after 2 weeks of Exos injection (Figure S2B). Importantly, obese ATM-Exos treatment led to impaired glucose tolerance and insulin sensitivity compared to either lean ATM-Exos treated mice or NCD control animals, as measured by glucose and insulin tolerance tests (Figures 2A and 2B). In addition, treatment with obese ATM-Exos led to increased glucose-stimulated insulin levels (GSIS; Figure S2C). In contrast, injection of lean ATM-Exos had no effect on glucose or insulin tolerance in NCD recipient mice (Figures 2A and 2B).

To quantify the impact of obese ATM-Exos on insulin sensitivity and to identify tissue-specific responses in muscle, liver, and adipose tissue *in vivo*, we performed hyperinsulinemic-euglycemic clamp studies in the lean chow-fed recipients. Animals were treated with either obese ATM-Exos (for 2 weeks) or empty liposomes as controls. Compared to the NCD controls, administration of obese ATM-Exos significantly decreased systemic insulin sensitivity, as evidenced by a lower overall glucose infusion rate (GIR) (Figure 2C). In addition, obese ATM-Exos treatment led to decreased insulin-stimulated glucose disposal rates (IS-GDR) (a measurement of skeletal muscle insulin sensitivity) (Figure 2D). The ability of insulin to suppress both hepatic glucose production (HGP) and circulating free fatty-acid (FFA) levels was also reduced (Figures 2E and 2F). Consistent with these results, insulin signaling was reduced in these tissues, as evidenced by decreased insulin-stimulated phosphorylation of AKT (Figures 2G–2I). Expression of PPARγ, which can promote insulin sensitivity, was also decreased after obese ATM-Exos administration (Figures S2D–S2F). This was accompanied by a corresponding decrease in adipocyte or muscle GLUT4 (a PPARγ target gene) expression (Figures S2D and S2E). Thus, ATMs from obese animals produce miRNA-containing Exos that can impair *in vivo* insulin sensitivity in these three major insulin target tissues.

## Obese ATM-Exosomal miRNAs Impair Cellular Insulin Sensitivity

Given the marked *in vivo* effects of obese ATM-Exos, we conducted *in vitro* studies of insulin action in adipocytes, myocytes, and hepatocytes.

As seen in Figures 3A and 3B, treatment of 3T3-L1 adipocytes and L6 myocytes with obese ATM-Exos led to a marked reduction in insulin-stimulated glucose uptake. In WT primary hepatocytes, glucagon treatment stimulated hepatic glucose output, and this effect was completely inhibited by insulin (Figure 3C). Strikingly, treatment of primary hepatocytes with obese ATM-Exos blocked the effect of insulin to suppress glucagon-stimulated HGP (Figure 3C). In addition, we observed decreased insulin-stimulated phosphorylation of AKT after obese ATM-Exos treatment in all three insulin target cell types (Figures 3D–3F). Expression of PPARγ in these cells was also suppressed by obese ATM-Exos treatment, along with a concomitant reduction in GLUT4 expression in both adipocytes and myocytes (Figures S3A–S3C). Overall, these results are consistent with the impaired *in vivo* insulin sensitivity in NCD recipient mice after treatment with obese ATM-Exos.

To demonstrate that miRNAs are the key functional components in these Exos, we conducted small interfering RNA (siRNA) knockdown of Drosha (an essential polymerase for miRNA synthesis) in lipopolysaccharide (LPS)-induced M1 BMDMs (~80% efficiency) (Figures S3D and S3E). This prevents miRNA synthesis, leading to production of miRNA-depleted Exos (Figures S3F and S3G). Treatment of 3T3-L1 adipocytes with Exos

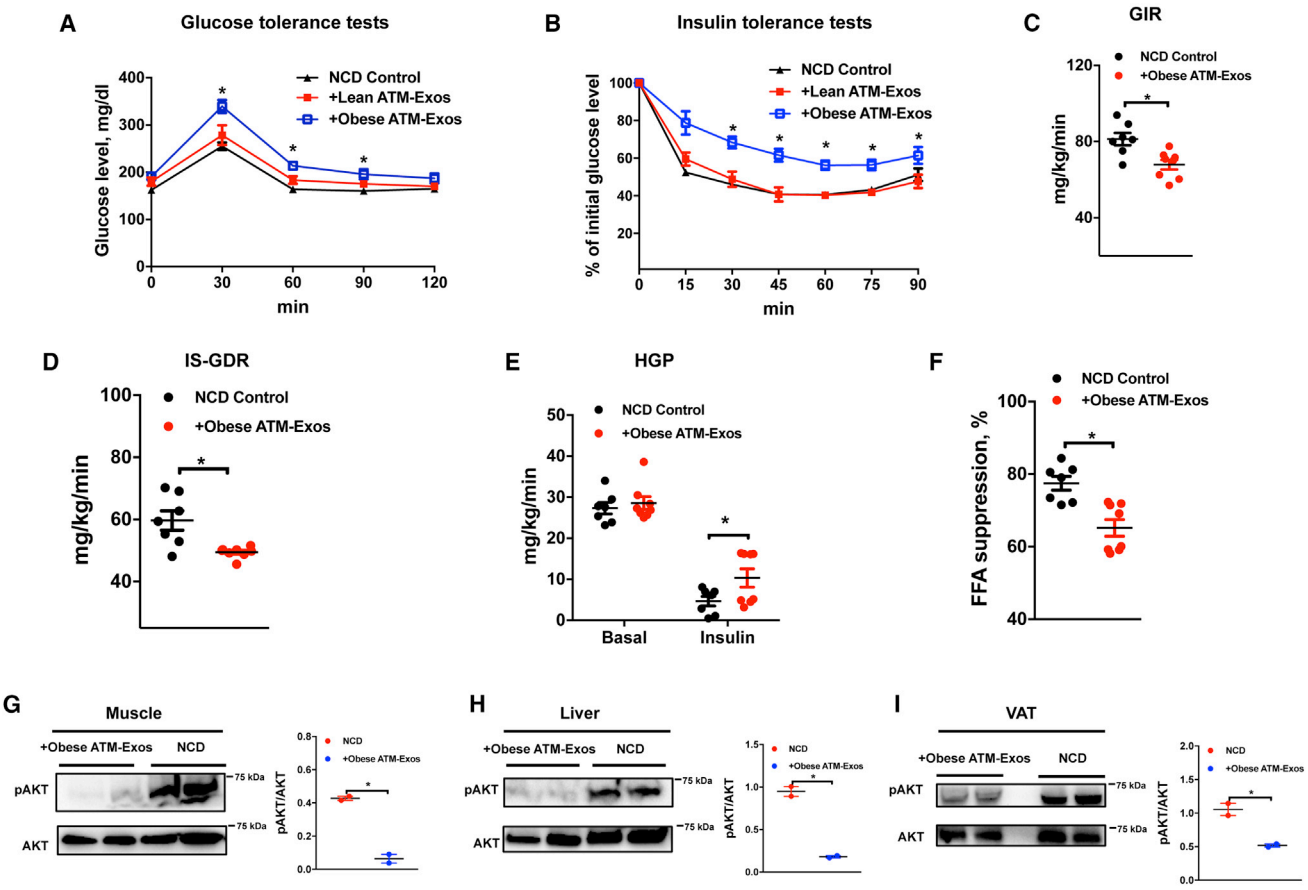


**Figure 2. Obese ATM-miRNA Containing Exos Cause Insulin Resistance**

(A and B) After 2 weeks of adoptive transfer of ATM exosomes (ATM-Exos), glucose tolerance tests (GTTs) (A) and insulin tolerance tests (ITTs) (B) were performed in normal chow diet (NCD)-fed WT recipient mice.

(C–F) Glucose infusion rate (GIR) (C), insulin-stimulated glucose disposal rate (IS-GDR) (D), hepatic glucose production (HGP) (E), and the percentage of suppression of free fatty-acid levels (FFA suppression) (F) during hyperinsulinemic-euglycemic clamp studies.

(G–I) AKT phosphorylation levels at S473 in skeletal muscle (G), liver (H), and VAT (I) were measured by western blot analysis after insulin injection. These blots are representative of 3 replicated independent experiments, each containing 2 samples.

Data are presented as mean ± SEM. n = 7 mice for NCD control group (A–F) and n = 8 mice for the other groups. *$p < 0.05$, 1-way ANOVA with Bonferroni's post-test (A and B) or Student's t test (C–F).

See also Figure S2.

isolated from control or Drosha-knockdown macrophages showed that the effect of M1 macrophage Exos to inhibit insulin-stimulated glucose uptake did not occur with miRNA-depleted M1 Exos (Figure 3G). These results indicate that miRNAs are responsible for the ability of macrophage-derived Exos to modulate insulin sensitivity.

## ATM-Derived Exos from Lean Animals Attenuate Obesity-Induced Insulin Resistance

Given the negative impact of obese ATM-Exos miRNAs on insulin action, we next evaluated whether exosomal miRNAs secreted from ATMs derived from lean animals could mitigate insulin resistance in obese recipient animals. We observed an efficient *in vivo* tissue uptake of transferred PKH26-labeled lean ATM-Exos, as measured by the appearance of PKH26 fluorescence in liver, VAT, and muscle of obese recipient mice (Figure S4A). A 2-week treatment of HFD/obese recipients with lean ATM-Exos led to near normalization of glucose and insulin tolerance (Figures 4A and 4B). The ability of lean ATM-Exos to improve insulin sensitivity in HFD recipients was confirmed by hyperinsulinemic-euglycemic clamp studies, as shown by increased GIR, increased IS-GDR, and an increased ability of insulin to suppress HGP (Figures 4C–4E). No difference in FFA levels was observed (Figure 4F). In contrast, treatment of obese recipient mice with obese ATM-Exos had only negligible effects (Figures 4A and 4B). Neither obese nor lean ATM-Exos treatment had any effect on body weight and GSIS (Figures S4B and S4C). Interestingly, whereas Thomou et al. (2017) recently showed that brown adipocytes can secrete Exos containing miR-99b, which suppresses hepatic FGF21 expression, we found no effect of obese or lean ATM-Exos on circulating FGF21 levels in lean or obese recipient mice (Figure S4D).

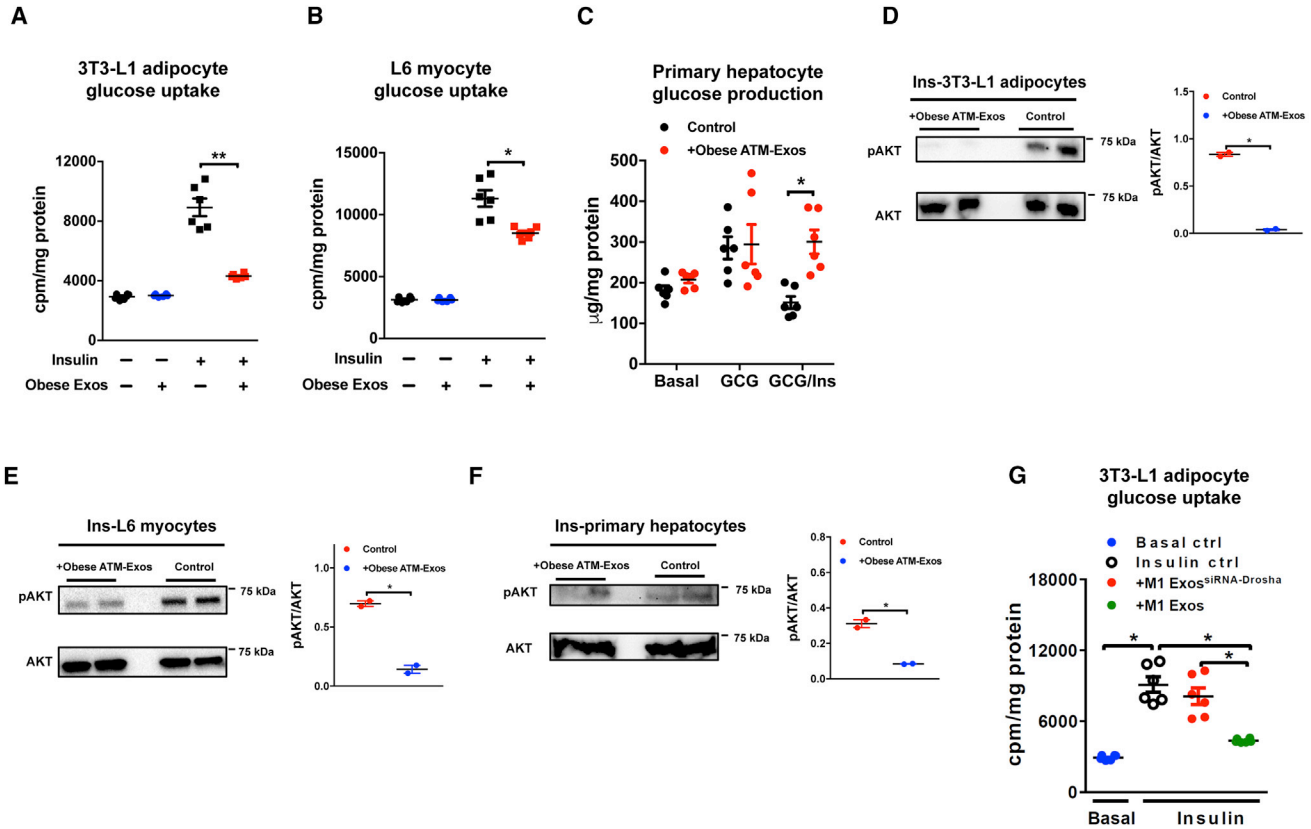


**Figure 3. Obese ATM-Exos Modulate Insulin Action in Target Cells through Exosomal miRNAs**

(A–C) Effect of obese ATM-Exos on glucose uptake in 3T3-L1 adipocytes (A) and L6 muscle cells (B) as well as glucose production in primary hepatocytes (C). (D–F) AKT phosphorylation levels in 3T3-L1 adipocytes, L6 muscle cells, and primary hepatocytes after treatment with obese ATM-Exos. These blots are representative of 3 replicated independent experiments, each containing 2 samples.

(G) Exos were collected from LPS-induced M1 BMDMs after siRNA-mediated knockdown of Drosha (M1 Exos$^{siRNA\text{-}Drosha}$) and then cultured with 3T3-L1 adipocytes. After 24 hr, adipocyte glucose uptake was measured.

Data are presented as mean ± SEM. n = 6 per group (A–C and G). *$p < 0.05$, **$p < 0.01$, Student's t test. Ins, insulin.

See also Figure S3.

Lean ATM-Exos treatment also enhanced insulin-stimulated AKT phosphorylation in insulin target tissues of HFD WT recipient mice (Figure S4E). In addition, after treatment with lean ATM-Exos, the inflammatory status of VAT was attenuated, as evidenced by reduced production of proinflammatory cytokines and phosphorylation of p65 (Figures S4F and S4G). Administration of lean ATM-Exos did not affect the population of ATMs in these HFD recipient mice (Figure S4H). Consistent with the improved *in vivo* insulin sensitivity, lean ATM-Exos treatment promoted insulin-stimulated glucose uptake in 3T3-L1 adipocytes and L6 muscle cells (Figures 4G and 4H). Taken together, these results suggest that ATM-secreted exosomal miRNAs produced in the lean state provide protection against obesity-induced insulin resistance.

## Obesity Induces Changes in ATM-Exo miRNA Expression

To assess obesity-induced changes in expression of ATM-Exo miRNAs, we conducted deep sequencing of small RNAs from lean and obese ATM-Exos. Over 500 miRNAs were identified in ATM-Exos (Figure 5A; Table S1). We also identified a set of miRNAs that are differentially expressed in obese versus lean ATM-Exos. Among these differentially expressed miRNAs, Figure 5A shows the 20 miRNAs with the most significant (fold change > 2, $p < 0.05$) abundance difference between lean and obese ATM-Exos.

Among the identified miRNAs, miR-155 reportedly influences adipocyte differentiation through direct suppression of PPARγ (Chen et al., 2013). It has also been demonstrated that proinflammatory macrophages preferentially produce miR-155 (Ortega et al., 2015). Our results show that ATMs from obese mice expressed ~3-fold greater intracellular levels of miR-155 (Figure 5B), which leads to increased levels of miR-155 present in the Exos (Figure 5C). Incubation of 3T3-L1 adipocytes, L6 muscle cells, and primary hepatocytes, with obese ATM-Exos also led to a significant increase in miR-155 abundance within these cells, while treatment with lean ATM-Exos led to small or non-significant effects (Figures 5D–5F). Consistent with these results, miR-155 expression was markedly increased in miR-155KO primary adipocytes and hepatocytes after obese ATM-Exos

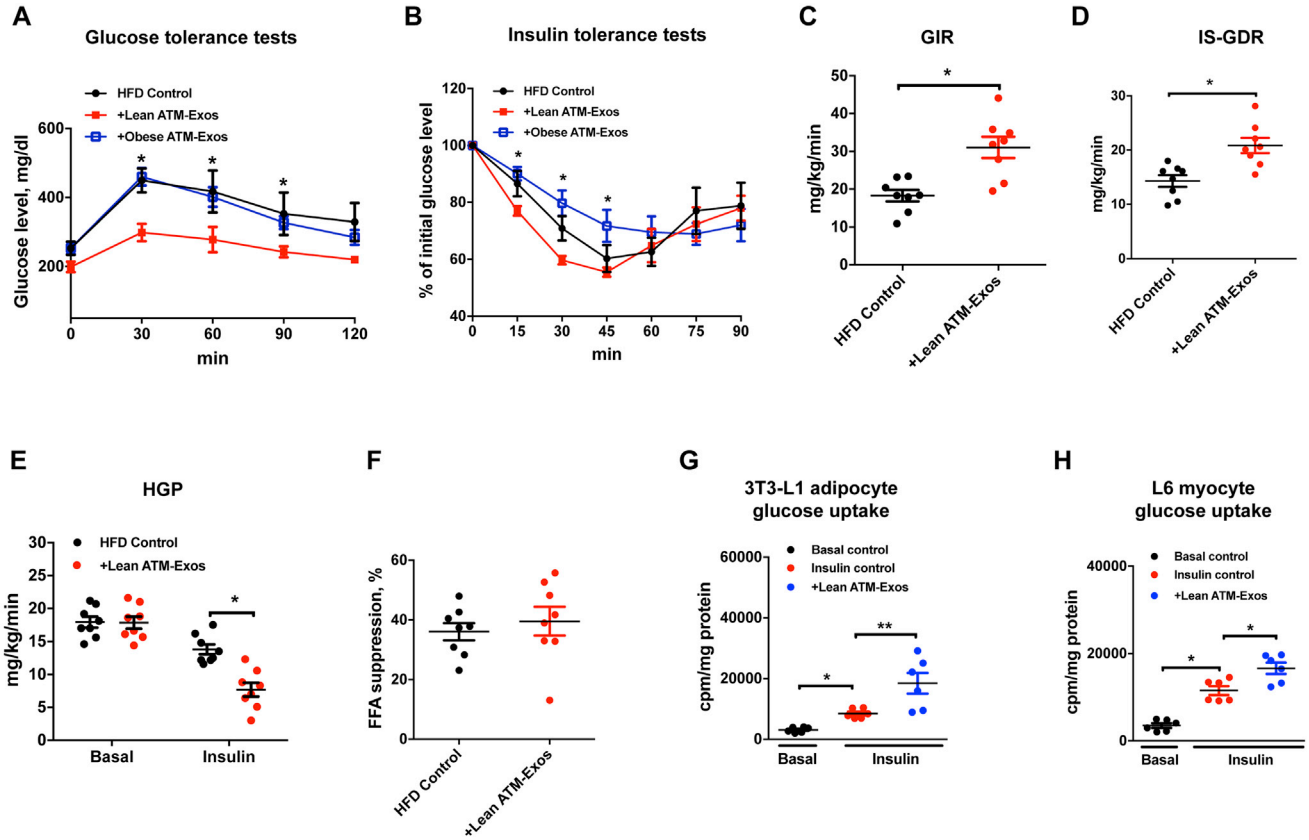


**Figure 4. Lean ATMs-Exos Attenuate Obesity-Induced Insulin Resistance**

(A and B) GTTs (A) and ITTs (B) in HFD-fed WT recipient mice after 2 weeks of adoptive transfer of ATM-Exos.

(C–F) GIR (C), IS-GDR (D), HGP (E), and FFA suppression (F) during hyperinsulinemic euglycemic clamp studies.

(G and H) The effects of lean ATM-Exos on glucose uptake in 3T3-L1 adipocytes and L6 myocytes.

Data are presented as mean ± SEM. n = 8 mice per group (A–F); n = 6 per group (G and H). *$p < 0.05$, **$p < 0.01$, 1-way ANOVA with Bonferroni's post-test (A and B) or Student's t test (C–H).

See also Figure S4.

treatment (Figure S5A). In addition, *in vivo* treatment of lean mice with obese ATM-Exos led to accumulation of miR-155 in primary adipocytes isolated from the treated recipient animals (Figure S5B). This led to suppression of the miR-155 target gene, PPARγ, as well as several downstream PPARγ-target genes (Figure S5C).

## MiR-155 Impairs Cellular Insulin Signaling

To further explore the mechanisms by which obese ATM-Exos induce insulin resistance, we determined the effects of miR-155 on insulin signaling. Overexpression of miR-155 significantly reduced insulin-stimulated glucose uptake in 3T3-L1 adipocytes and L6 muscle cells, and this was accompanied by decreased expression of the miR-155 target gene PPARγ (Figures 6A, 6B, 6D, and S5D–S5F). Concomitantly, expression of GLUT4, a known PPARγ target gene, was also decreased in these cells (Figure 6D). In primary hepatocytes, transfection of the miR-155 mimic impaired the suppressive effect of insulin on glucose production, along with decreased PPARγ expression (Figures 6C and 6D). Furthermore, insulin-induced phosphorylation of AKT was decreased in adipocytes, myocytes, and hepatocytes by miR-155 overexpression (Figure S5G).

Within the RISC, miRNAs bind to a protein termed Argonaut (Ago) and the bound miRNAs then recruit their target mRNAs into this complex. To further show that PPARγ is a direct target of miR-155, we immunoprecipitated Ago and its bound RNAs. qPCR analysis shows that overexpression of miR-155 led to an increase in the amount of *Pparg* bound to Ago protein (Figure 6E).

We also assessed whether activation of PPARγ could rescue the cellular insulin resistance induced by miR-155. Interestingly, treatment of cells with the PPARγ agonist rosiglitazone (Rosi) attenuated the suppressive effect of miR-155 on insulin-stimulated glucose uptake in 3T3-L1 adipocytes and L6 muscle cells (Figure 6F).

## ATM-Exosomal miR-155 Promotes Obesity-Induced Insulin Resistance

Given that miR-155 inhibited cellular insulin signaling, we evaluated the effects of miR-155 on obesity-induced insulin

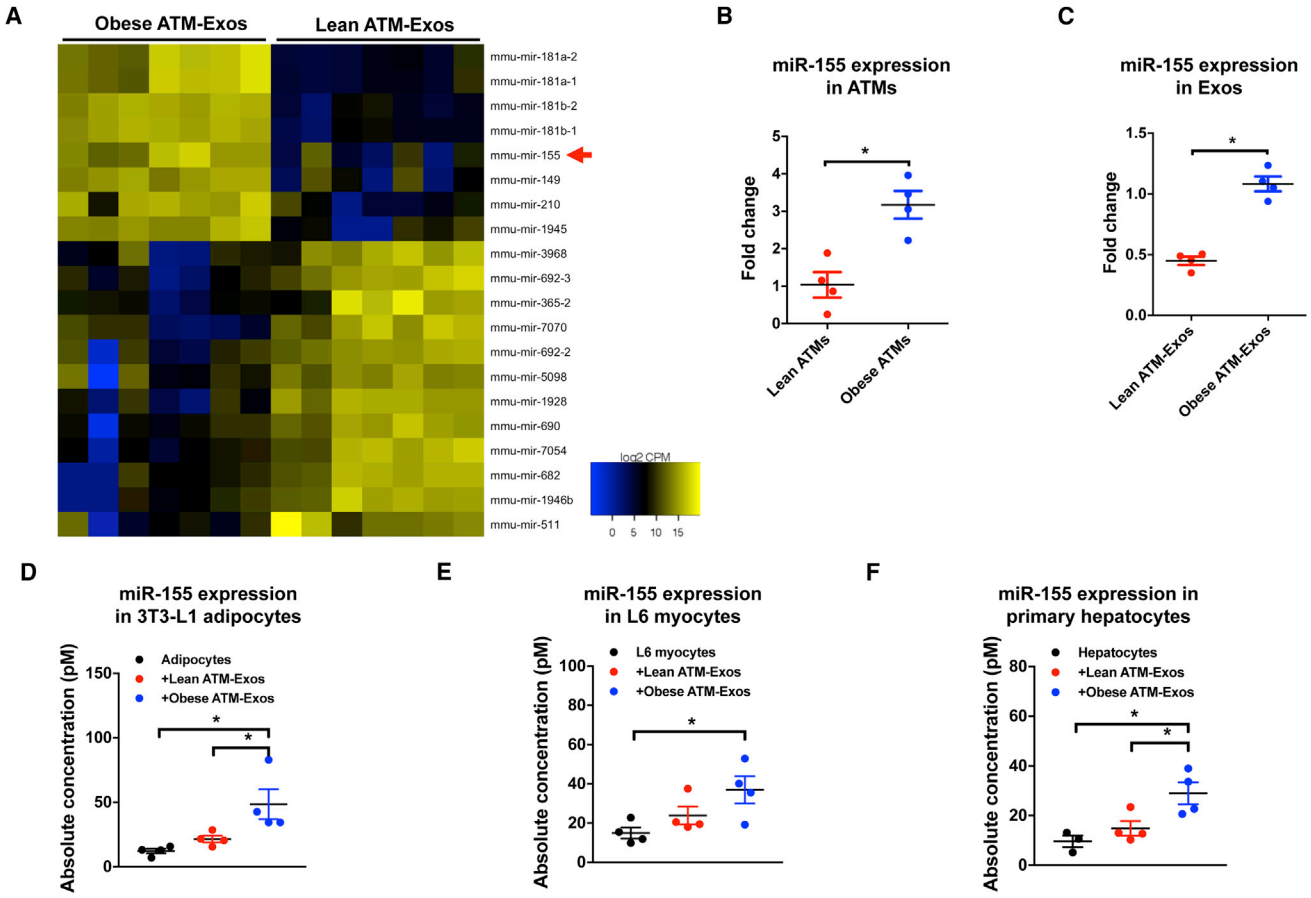


**Figure 5. Obesity Leads to Changes in ATM-Exo miRNA Profiles**

(A) Differential expression level of exosomal miRNAs between lean ATMs and obese ATMs. MiR-155 is one of the exosomal miRNAs with markably greater abundance in obese ATM-Exos compared to lean ATM-Exos.

(B) Expression level of miR-155 in lean ATMs and obese ATMs.

(C) MiR-155 abundance in Exos secreted by lean ATMs and obese ATMs.

(D–F) After 24 hr of lean or obese ATM-Exos treatment, the levels of miR-155 in adipocytes (D), L6 muscle cells (E), and primary hepatocytes (F) were measured by qPCR analysis. Data were normalized to levels of U6 (cellular) or total protein of Exos.

Data are presented as mean ± SEM. n = 4 per group (B)–(F). *$p < 0.05$, Student's t test.

See also Figure S5 and Table S1.

resistance *in vivo*. MiR-155 knockout (miR-155KO) mice were fed a HFD for 12 weeks. As predicted from our *in vitro* results, depletion of miR-155 attenuated obesity-induced glucose intolerance and systemic insulin resistance, compared to HFD-WT mice (Figures 7A and 7B).

To assess specifically whether WT bone marrow-derived cells expressing miR-155 can mediate systemic insulin resistance, we performed bone marrow transplantation experiments. To generate chimeric mice, irradiated miR-155KO recipient mice were adoptively transferred with bone marrow cells from either GFP-WT donor mice (BMT-WT) or miR-155KO donor mice (BMT-miR-155KO).

After 8 weeks, the engraftment of GFP donor cells in irradiated recipient mice was confirmed by the presence of donor-derived GFP expressing CD45+ peripheral blood cells (PBCs), as well as miR-155 expression in PBCs (Figures S6A and S6B). All miR-155KO recipient mice were subsequently treated with HFD. After 20 weeks of HFD feeding, recipient mice displayed similar body weight and GSIS (Figures S6C and S6D), as well as comparable populations of ATMs (Figure S6E). Glucose tolerance and insulin sensitivity were impaired in BMT-WT mice, compared to BMT-miR-155KO mice (Figures 7C and 7D), but were not as severe as in WT HFD mice.

To assess further the differences in cellular insulin responses between BMT-WT and BMT-miR-155KO mice, we measured expression of miR-155 and its target gene PPARγ in primary adipocytes and hepatocytes (Figures 7E and 7F). MiR-155 abundance was partially restored in both types of primary cells after transplantation of WT GFP donor cells (Figure 7E), leading to a decrease in the expression of PPARγ (Figure 7F). Accumulation of miR-155 also caused impaired cellular insulin signaling, as measured by reduced insulin-stimulated glucose uptake in primary adipocytes and improved insulin-induced suppression of hepatic glucose output in primary hepatocytes

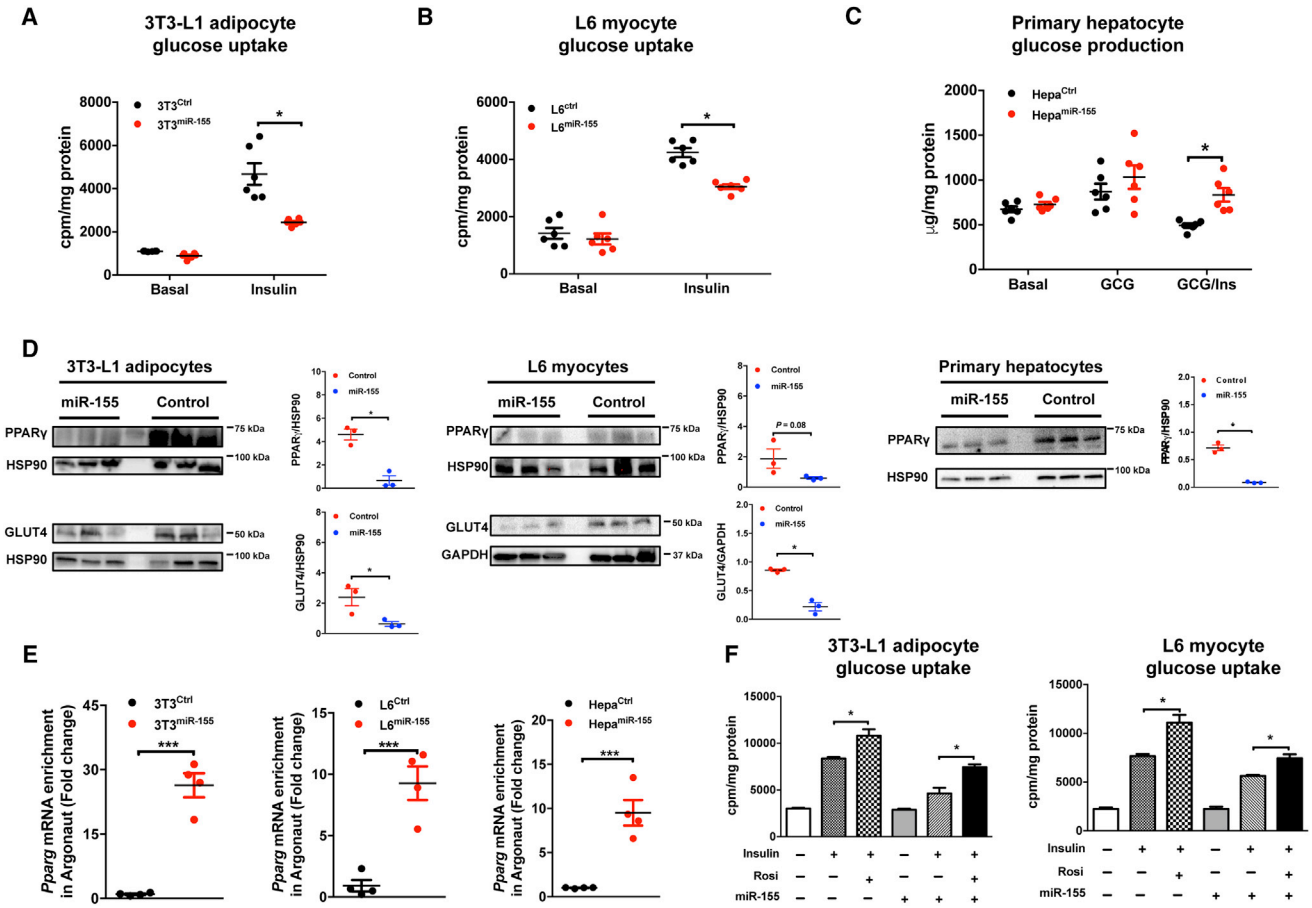


**Figure 6. MiR-155 Impairs Cellular Insulin Action**

(A–C) Glucose uptake in 3T3-L1 adipocytes (A) and L6 muscle cells (B) as well as glucose production by primary hepatocytes (C) after 24 hr transfection with a miR-155 mimic.

(D) After overexpression of miR-155, the expression of the target gene PPARγ was measured by western blot analysis. The expression of GLUT4, a PPARγ-induced gene, was also measured in 3T3-L1 adipocytes and L6 cells. In the western blot analyses, the exposure time to detect PPARγ in 3T3-L1 adipocytes, L6 myocytes, and primary hepatocytes was 100 s, 480 s, and 440 s, respectively. The exposure time to detect GLUT4 in 3T3-L1 adipocytes and L6 myocytes was 80 s and 60 s, respectively. These blots are representative of 3 replicated independent experiments, each containing 3 samples.

(E) The abundance of *Pparg* mRNA bound with argonaut protein in recipient cells after overexpression of miR-155.

(F) The effects of rosiglitazone (Rosi) on recovery of glucose uptake in 3T3-L1 adipocytes and L6 muscle cells with overexpression of miR-155.

Data are presented as mean ± SEM. n = 6 per group (A–C and F) and n = 4 per group (E). *$p < 0.05$, Student's t test. GCG, glucagon. Ctrl, control.

See also Figure S5.

(Figures 7G and 7H). These suppressive effects of miR-155 on insulin action were confirmed by finding reduced phosphorylation of AKT in primary adipocytes and hepatocytes of BMT-WT mice (Figure S6F). These primary adipocyte and hepatocyte preparations displayed minimal (adipocytes) or non-detectable (hepatocytes) macrophage contamination, as shown by measurement of *Emr1* and miR-223 expression or flow cytometry analysis (Figures S6G–S6I).

## DISCUSSION

In this study, we have shown that miRNA-containing ATM-Exos can modulate systemic insulin and glucose tolerance by directly affecting cellular insulin signaling. Thus, when lean insulin sensitive mice are treated with obese ATM-Exos they develop systemic insulin resistance and glucose intolerance. In contrast, treatment of obese insulin resistant mice with lean ATM-Exos leads to near normalization of glucose tolerance with an improvement in systemic insulin sensitivity. ATM-Exos treatment had no effect on body weight, and after *in vivo* administration, uptake of ATM-Exos can be demonstrated in liver, muscle, and fat. *In vitro* experiments show that treatment with obese ATM-Exos directly causes decreased insulin signaling in adipocytes, myocytes, and hepatocytes, whereas lean ATM-Exos have the opposite effect and improve cellular insulin sensitivity. These studies suggest that miRNAs within secreted ATM-Exos can be taken up by insulin target cells and directly affect glucose homeostasis and insulin sensitivity.

Secreted extracellular vesicles were harvested from macrophage conditioned media by differential centrifugation. We

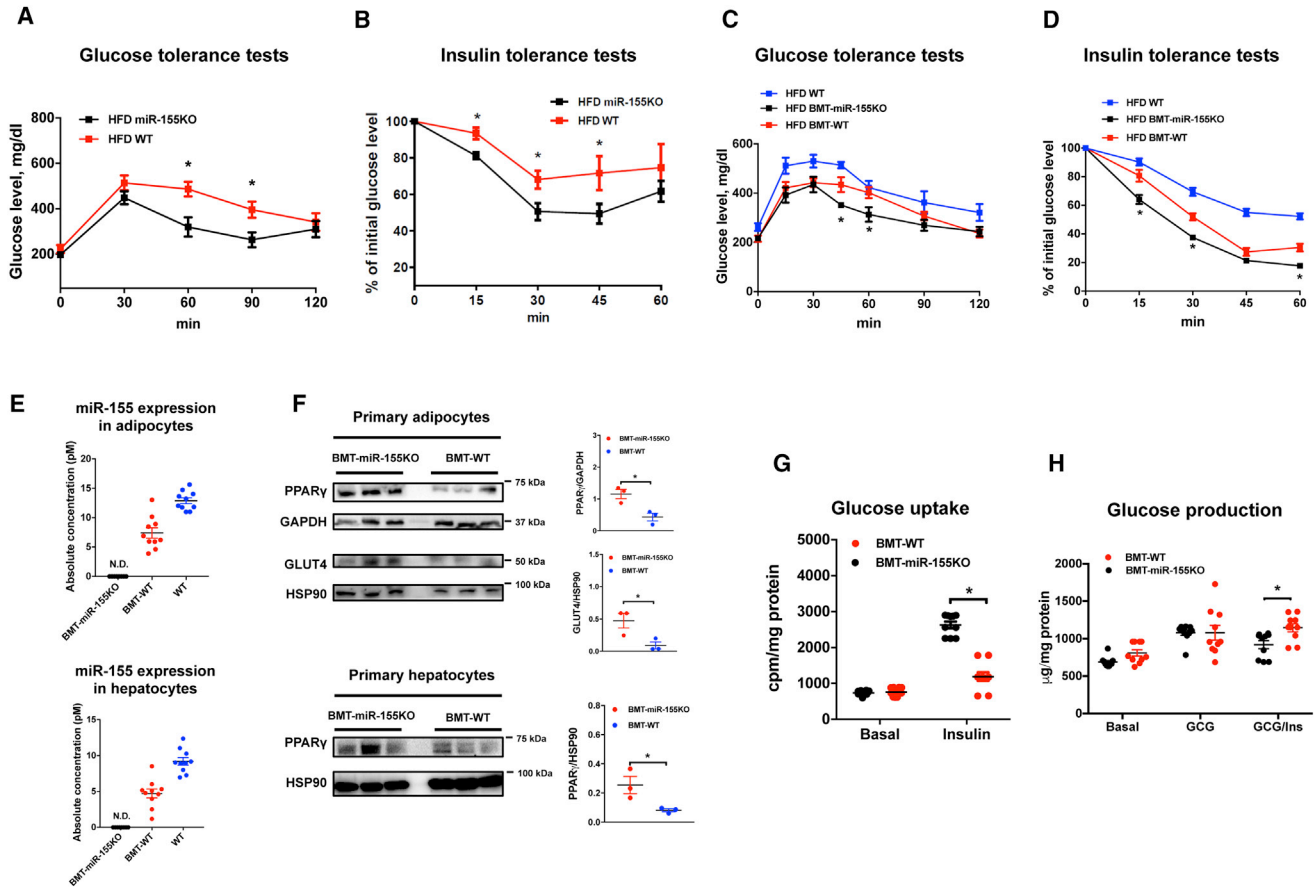


**Figure 7. WT Bone Marrow Reconstitution in miR-155KO Mice Promotes Obesity-Induced Insulin Resistance**

(A and B) GTTs and ITTs from HFD-fed WT and miR-155KO mice. HFD-fed miR-155KO recipient mice received miR-155KO (BMT-miR-155KO) or WT (BMT-WT) bone marrow cells.

(C and D) After bone marrow transplantation and 20 weeks HFD feeding, GTTs and ITTs were performed on miR-155KO recipient mice.

(E) MiR-155 abundance in primary adipocytes and hepatocytes of the miR-155KO recipient mice was examined by qPCR analysis.

(F) The abundance of miR-155 target gene PPARγ was measured in primary adipocytes and hepatocytes in miR-155KO recipient mice after bone marrow transplantation. GLUT4 expression was also measured in primary adipocytes. In the western blot analyses, the exposure time to detect PPARγ in primary adipocytes and hepatocytes was 120 s and 550 s, respectively. The exposure time to detect GLUT4 protein band was 150 s. These blots are representative of 3 replicated independent experiments, each containing 3 samples.

(G and H) Glucose uptake in primary adipocytes and glucose production in primary hepatocytes were measured after bone marrow transplantation.

Data are presented as mean ± SEM. n = 10 mice per group (A–E) and n = 10 per group (G–H). *$p < 0.05$, 1-way ANOVA with Bonferroni's post-test (A–D) or Student's t test (G and H).

See also Figure S6.

identified these extracellular vesicles as Exos with a diameter of 30-100 nanometers by electromicroscopy, NanoSight analysis, and measurement of the exosomal membrane markers TSG101, syntenin 1, CD63, and CD9 (Kowal et al., 2016; Zhang et al., 2015a). Several methods were used to demonstrate direct transfer of exosomal miRNAs into insulin target cells. First, we transfected macrophages with Cy3-labeled miR-223 and applied these cells to the upper chamber of a transwell dish with 3T3-L1 adipocytes in the lower chamber. Using this approach, fluorescently labeled miR-223 was readily detected in the adipocytes with a several fold increase in expression. In a second approach, ATM-derived Exos were directly labeled with PKH26 fluorescent dye. 3T3-L1 adipocytes were treated with these labeled Exos and uptake of the fluorescent label into adipocytes was directly demonstrated. This was also accompanied by increased expression of macrophage miR-223 in the adipocytes and the effect was suppressed by prior treatment of the ATMs with the EV secretion inhibitor GW4869. We also showed a robust increase in miR-155 expression when miR-155KO adipocytes and hepatocytes were treated ex vivo with obese ATM-Exos. Taken together, these experiments show that ATMs produce miRNA-containing Exos and that the miRNA cargo can be directly transferred into adipocytes *in vitro*. Our *in vivo* studies are consistent with this concept and show that treatment of mice with either lean or obese PKH26 labeled Exos leads to retention of these Exos in liver, muscle, and VAT of recipient mice.

Our ATM exosomal preparations were made using published techniques (Fong et al., 2015; Zhang et al., 2015b), and these

vesicle preparations were characterized in detail with respect to expression of reported exosome protein markers (Figure 1B), size (Figure 1C), and miRNA content (Figure 5). In addition, we performed density gradient centrifugation of our exosomal preparations and found that the great majority of the proteins (>90%), exosomal markers, and miRNA (> 97%), as exemplified by miR-155, were contained in fractions 3 and 4 (Figures S1D–S1F), as reported by Kowal et al. (2016). The exact characterization of these extracellular vesicles is presented in Figures 1 and S1. It is clear that our ATM Exo preparations are miRNA-containing ATM-derived EVs, and based on a comparison of the characterization of these vesicles to the published literature, we think it is reasonable to refer to them as ATM-derived Exos. We prefer this term over exosome-like or ATM-derived EVs, since it more clearly captures the concepts presented in this manuscript. We recognize that this is an operational definition and that this field is evolving. However, the characterization data provided in Figures 1 and S1 provide a biochemical and structural characterization of our exosomal preparations.

The concept that exosomal miRNAs can be transferred to other cell types is supported by *in vitro* data showing that endothelial derived Exos can target vascular cells (Ismail et al., 2013). In addition, Exos secreted from macrophages can be taken up by circulating monocytes (Ismail et al., 2013). With respect to metabolic effects, Jordan et al. have reported that obesity induces expression of miR-143 in the liver and that this miRNA blunts hepatic insulin sensitivity by suppression of its target gene ORP8 (Jordan et al., 2011). In adipocytes, miR-222 expression is increased in obesity and can impair insulin sensitivity by inhibiting ER$\alpha$ and GLUT4 expression (Shi et al., 2014). In our current studies, a 2-week treatment of lean recipient mice with obese ATM-Exos led to glucose intolerance and insulin resistance in muscle, liver, and adipose tissue. Reverse experiments in which insulin resistant obese mice were treated with lean ATM-Exos showed a marked effect to normalize glucose tolerance and insulin sensitivity in the obese recipient mice. *In vitro* studies showed that treatment with obese ATM-Exos led to decreased insulin-stimulated glucose transport in adipocytes and myocytes, while lean ATM-Exos treatment improved insulin sensitivity. These *in vitro* results are consistent with a report from Zhang et al. (2015c) showing that M1 THP-1 cell-derived EVs can impair insulin responses in human adipocytes. Our results also demonstrated that it is the miRNAs within the Exos that caused these effects on insulin signaling. Thus, when siRNA was used to deplete Drosha (a key protein in miRNA production) from proinflammatory macrophages prior to harvesting of Exos, the miRNA-depleted Exos had no effect to inhibit insulin-stimulated glucose transport.

MiRNAs can theoretically have more than one mRNA target, and there could be more than one miRNA directed against an mRNA species (Bartel, 2009). To further understand which of the exosomal miRNAs, or sets of miRNAs, are responsible for the metabolic phenotypes we have observed, we sequenced the miRNAs in the obese and lean ATM-Exos. This analysis revealed that several hundred miRNA species were present within ATM-Exos. In addition, there were a number of differentially expressed miRNAs between the lean and obese state and it is thought that only relatively high expressing miRNAs have biologic effects. In analyzing these differentially expressed miRNAs, miR-155 emerged as a highly expressed candidate of interest, because it has been shown that miR-155 can influence adipocyte differentiation by repressing PPAR$\gamma$ (Chen et al., 2013). Given the obvious importance of PPAR$\gamma$ for adipocyte function and systemic metabolism (Sugii et al., 2009; Tontonoz et al., 1994; Tontonoz and Spiegelman, 2008), we conducted further studies in miR-155KO mice and bone marrow transplant chimeras. Interestingly, miR-155KO mice were protected from HFD-induced insulin resistance and glucose tolerance, with no change in body weight. Transplantation of WT BM into miR-155KO mice mitigated the insulin sensitive/glucose tolerant phenotype and, as expected, we found that miR-155 can down-regulate PPAR$\gamma$ expression. This indicates that miR-155 contributes to the insulin resistant, glucose intolerant state conferred by obese ATM-Exos. However, it is unlikely that miR-155 is the sole explanation for the differences in insulin sensitivity in Exos treated mice, as there are most likely other miRNAs within these Exos that play important functional roles. In addition, it is possible that multiple miRNAs within the ATM-Exos could work in a coordinated way to induce the insulin resistant and insulin sensitive phenotypes that we have observed. Future work will be necessary to demonstrate the full set of ATM-Exos miRNAs causing metabolic effects. Searching NCBI, as well as other publicly available datasets (such as http://www.type2diabetesgenetics.org) revealed no evidence for miR-155-associated single-nucleotide polymorphisms (SNPs) connected to metabolic diseases. This result is not inconsistent with our overall hypotheses, since our concept is that inflammation with macrophage accumulation in adipose tissue is the underlying etiology and that the miRNAs appear in the obese ATM Exos as a function of the proinflammatory profile of the accumulated M1-like macrophages.

Previous reports have assessed blood miRNA content in normal, obese, or type 2 diabetic individuals (Iacomino et al., 2016; Ortega et al., 2014; Pescador et al., 2013; Zampetaki et al., 2010). Several different miRNAs have been reported as differentially expressed across disease states. However, within these papers, the specific differentially expressed miRNAs are not concordant and different patterns have been reported. Clearly, the potential of circulating miRNAs as biomarkers for metabolic diseases is of great interest (Guay and Regazzi, 2013) and additional work is needed to define consistent patterns, which differentiate normal versus metabolic disease.

Ortega et al. reported that Exo miRNAs are released into conditioned media after treating THP1 macrophages with LPS (Ortega et al., 2015). Of the 223 miRNAs they detected in the conditioned media, 138 were also present in our ATM-Exo miRNA dataset. A recent paper by Thomou et al. (2017) demonstrated the presence of 653 miRNAs expressed in serum-derived Exos from WT mice. The authors also studied adipocyte-specific Dicer KO mice in order to deplete adipocyte-derived miRNAs (Thomou et al., 2017). In their paper, the principal finding was that brown adipocytes release Exos containing miR-99b, which, in turn, inhibits FGF21 expression in the liver (Thomou et al., 2017). The authors suggest that these changes in FGF21 give rise to the *in vivo* phenotype of the adipocyte Dicer KO mice. In our studies, FGF21 levels were unaffected by ATM-Exo

administration (Figure S4D) and miR-99b was the same between lean and obese ATM-Exos (adjusted p value = 0.115; Table S1). Of all the 422 miRNAs depleted by adipocyte-specific Dicer KO, only 79 were present in our ATM-Exos, and among our top 30 differentially expressed miRNAs between lean and obese ATM-Exos, only 6 were depleted in the adipocyte-specific Dicer KO mice (Thomou et al., 2017). This indicates that marked differences exist in the miRNA repertoires between ATMs and adipocytes within adipose tissue. Thus, ATMs and adipocytes, which both reside within adipose tissue, release Exos containing different miRNA cargo and elicit phenotypes through completely different mechanisms.

In summary, we find that ATMs secrete miRNA containing Exos that influence metabolism. Treatment with obese ATM-Exos leads to *in vivo* and *in vitro* insulin resistance, whereas, lean ATM-Exos produce a state of insulin sensitivity in obese mice and enhance insulin signaling *in vitro*. It is recognized that chronic tissue inflammation with proinflammatory macrophage accumulation, particularly in adipose tissue and liver, is an important feature of obesity-induced insulin resistance (Lackey and Olefsky, 2016) and several soluble macrophage-derived factors have been identified which can impair insulin signaling (Li et al., 2015, 2016). Based on these studies, we suggest that ATM-Exo miRNAs, represent a paracrine and endocrine signaling system, whereby proinflammatory and anti-inflammatory ATMs can influence metabolic events in distant tissues. It will be of interest to determine whether Exos produced by other tissues, such as β cells, hepatocytes, or myocytes, can have metabolic effects.

## STAR★METHODS

Detailed methods are provided in the online version of this paper and include the following:

- KEY RESOURCES TABLE
- CONTACT FOR REAGENT AND RESOURCE SHARING
- EXPERIMENTAL MODEL AND SUBJECT DETAILS
  - Animal care and use
- METHODS DETAILS
  - Glucose tolerance and insulin tolerance tests and hyperinsulinemic-euglycemic clamp studies
  - In vivo insulin-stimulated AKT phosphorylation assay
  - Isolation of stromal cells from visceral adipose tissue
  - Adipose tissue macrophage isolation
  - Primary pre-adipocyte isolation and adipocyte differentiation
  - Exosome purification and characterization
  - Electron microscopy
  - In vivo and in vitro exosome treatment
  - miRNA mimic or siRNA transfection
  - Argonaut-RNA co-immunoprecipitation assay
  - Co-culture assay
  - Flow cytometry analysis
  - Glucose uptake assay
  - Glucose output assay
  - Western blot analysis
  - RNA extraction and miRNA RT-qPCR assay
  - Bone marrow transplantation
- QUANTIFICATION AND STATISTICAL ANALYSIS
  - Study approval

## SUPPLEMENTAL INFORMATION

Supplemental Information includes six figures and one table and can be found with this article online at http://dx.doi.org/10.1016/j.cell.2017.08.035.

## AUTHOR CONTRIBUTIONS

W.Y. designed the studies and performed most of the experiments; M.R. performed hyperinsulinemic-euglycemic clamp studies; G.B. performed isolation of primary hepatocytes and glucose output assays; J.M. Ofrecio performed ELISA and genotyping; A.B. performed bioinformatics analysis; J.W. and A.H.-C. assisted with the tissue collection; P.L. assisted with the bone marrow transplantation assay; Y.D. and W.F. performed the histology analysis; J.B.S. performed the primary pre-adipocyte isolation and adipocyte differentiation; and W.Y. and J.M. Olefsky analyzed and interpreted the data, supervised the project, and co-wrote the manuscript.

## ACKNOWLEDGMENTS

This study was funded by the American Heart Association (16POST31350039 to W.Y.), the National Natural Science Foundation of China (81600610 to W.Y.), the UCSD/UCLA Diabetes Research Center Pilot and Feasibility grant (P30 DK063491 to W.Y.), a UC San Diego Clinical and Translational Research Institute grant (UL1TR001442 to A.B.), and the U.S. National Institute of Diabetes and Digestive and Kidney Diseases (DK033651, DK074868, DK063491, and DK09062 to J.M. Olefsky).

Received: April 12, 2017
Revised: July 3, 2017
Accepted: August 20, 2017
Published: September 21, 2017

## REFERENCES

Ameres, S.L., Martinez, J., and Schroeder, R. (2007). Molecular basis for target RNA recognition and cleavage by human RISC. Cell *130*, 101–112.

Bang, C., Batkai, S., Dangwal, S., Gupta, S.K., Foinquinos, A., Holzmann, A., Just, A., Remke, J., Zimmer, K., Zeug, A., et al. (2014). Cardiac fibroblast-derived microRNA passenger strand-enriched exosomes mediate cardiomyocyte hypertrophy. J. Clin. Invest. *124*, 2136–2146.

Bartel, D.P. (2004). MicroRNAs: genomics, biogenesis, mechanism, and function. Cell *116*, 281–297.

Bartel, D.P. (2009). MicroRNAs: target recognition and regulatory functions. Cell *136*, 215–233.

Brennecke, J., Stark, A., Russell, R.B., and Cohen, S.M. (2005). Principles of microRNA-target recognition. PLoS Biol. *3*, e85.

Chen, Y., Siegel, F., Kipschull, S., Haas, B., Fröhlich, H., Meister, G., and Pfeifer, A. (2013). miR-155 regulates differentiation of brown and beige adipocytes via a bistable circuit. Nat. Commun. *4*, 1769.

Chen, Y., Buyel, J.J., Hanssen, M.J., Siegel, F., Pan, R., Naumann, J., Schell, M., van der Lans, A., Schlein, C., Froehlich, H., et al. (2016). Exosomal microRNA miR-92a concentration in serum reflects human brown fat activity. Nat. Commun. *7*, 11420.

Costa-Silva, B., Aiello, N.M., Ocean, A.J., Singh, S., Zhang, H., Thakur, B.K., Becker, A., Hoshino, A., Mark, M.T., Molina, H., et al. (2015). Pancreatic cancer exosomes initiate pre-metastatic niche formation in the liver. Nat. Cell Biol. *17*, 816–826.

De Taeye, B.M., Novitskaya, T., McGuinness, O.P., Gleaves, L., Medda, M., Covington, J.W., and Vaughan, D.E. (2007). Macrophage TNF-alpha contributes to insulin resistance and hepatic steatosis in diet-induced obesity. Am. J. Physiol. Endocrinol. Metab. *293*, E713–E725.

Deng, Z.B., Poliakov, A., Hardy, R.W., Clements, R., Liu, C., Liu, Y., Wang, J., Xiang, X., Zhang, S., Zhuang, X., et al. (2009). Adipose tissue exosome-like vesicles mediate activation of macrophage-induced insulin resistance. Diabetes *58*, 2498–2505.

Dominguez, H., Storgaard, H., Rask-Madsen, C., Steffen Hermann, T., Ihlemann, N., Baunbjerg Nielsen, D., Spohr, C., Kober, L., Vaag, A., and Torp-Pedersen, C. (2005). Metabolic and vascular effects of tumor necrosis factor-alpha blockade with etanercept in obese patients with type 2 diabetes. J. Vasc. Res. *42*, 517–525.

Fong, M.Y., Zhou, W., Liu, L., Alontaga, A.Y., Chandra, M., Ashby, J., Chow, A., O'Connor, S.T., Li, S., Chin, A.R., et al. (2015). Breast-cancer-secreted miR-122 reprograms glucose metabolism in premetastatic niche to promote metastasis. Nat. Cell Biol. *17*, 183–194.

Guay, C., and Regazzi, R. (2013). Circulating microRNAs as novel biomarkers for diabetes mellitus. Nat. Rev. Endocrinol. *9*, 513–521.

Hirosumi, J., Tuncman, G., Chang, L., Görgün, C.Z., Uysal, K.T., Maeda, K., Karin, M., and Hotamisligil, G.S. (2002). A central role for JNK in obesity and insulin resistance. Nature *420*, 333–336.

Holland, W.L., Bikman, B.T., Wang, L.P., Yuguang, G., Sargent, K.M., Bulchand, S., Knotts, T.A., Shui, G., Clegg, D.J., Wenk, M.R., et al. (2011). Lipid-induced insulin resistance mediated by the proinflammatory receptor TLR4 requires saturated fatty acid-induced ceramide biosynthesis in mice. J. Clin. Invest. *121*, 1858–1870.

Hotamisligil, G.S., Arner, P., Caro, J.F., Atkinson, R.L., and Spiegelman, B.M. (1995). Increased adipose tissue expression of tumor necrosis factor-alpha in human obesity and insulin resistance. J. Clin. Invest. *95*, 2409–2415.

Hotamisligil, G.S., Peraldi, P., Budavari, A., Ellis, R., White, M.F., and Spiegelman, B.M. (1996). IRS-1-mediated inhibition of insulin receptor tyrosine kinase activity in TNF-alpha- and obesity-induced insulin resistance. Science *271*, 665–668.

Hulsmans, M., and Holvoet, P. (2013). MicroRNA-containing microvesicles regulating inflammation in association with atherosclerotic disease. Cardiovasc. Res. *100*, 7–18.

Iacomino, G., Russo, P., Stillitano, I., Lauria, F., Marena, P., Ahrens, W., De Luca, P., and Siani, A. (2016). Circulating microRNAs are deregulated in overweight/obese children: preliminary results of the I.Family study. Genes Nutr. *11*, 7.

Ismail, N., Wang, Y., Dakhlallah, D., Moldovan, L., Agarwal, K., Batte, K., Shah, P., Wisler, J., Eubank, T.D., Tridandapani, S., et al. (2013). Macrophage microvesicles induce macrophage differentiation and miR-223 transfer. Blood *121*, 984–995.

Johnnidis, J.B., Harris, M.H., Wheeler, R.T., Stehling-Sun, S., Lam, M.H., Kirak, O., Brummelkamp, T.R., Fleming, M.D., and Camargo, F.D. (2008). Regulation of progenitor cell proliferation and granulocyte function by microRNA-223. Nature *451*, 1125–1129.

Johnson, A.M., and Olefsky, J.M. (2013). The origins and drivers of insulin resistance. Cell *152*, 673–684.

Jordan, S.D., Krüger, M., Willmes, D.M., Redemann, N., Wunderlich, F.T., Brönneke, H.S., Merkwirth, C., Kashkar, H., Olkkonen, V.M., Böttger, T., et al. (2011). Obesity-induced overexpression of miRNA-143 inhibits insulin-stimulated AKT activation and impairs glucose metabolism. Nat. Cell Biol. *13*, 434–446.

Kahn, S.E., Hull, R.L., and Utzschneider, K.M. (2006). Mechanisms linking obesity to insulin resistance and type 2 diabetes. Nature *444*, 840–846.

Kosaka, N., Iguchi, H., Yoshioka, Y., Takeshita, F., Matsuki, Y., and Ochiya, T. (2010). Secretory mechanisms and intercellular transfer of microRNAs in living cells. J. Biol. Chem. *285*, 17442–17452.

Kowal, J., Arras, G., Colombo, M., Jouve, M., Morath, J.P., Primdal-Bengtson, B., Dingli, F., Loew, D., Tkach, M., and Théry, C. (2016). Proteomic comparison defines novel markers to characterize heterogeneous populations of extracellular vesicle subtypes. Proc. Natl. Acad. Sci. USA *113*, E968–E977.

Lackey, D.E., and Olefsky, J.M. (2016). Regulation of metabolism by the innate immune system. Nat. Rev. Endocrinol. *12*, 15–28.

Lewis, B.P., Shih, I.H., Jones-Rhoades, M.W., Bartel, D.P., and Burge, C.B. (2003). Prediction of mammalian microRNA targets. Cell *115*, 787–798.

Lewis, B.P., Burge, C.B., and Bartel, D.P. (2005). Conserved seed pairing, often flanked by adenosines, indicates that thousands of human genes are microRNA targets. Cell *120*, 15–20.

Li, P., Oh, D.Y., Bandyopadhyay, G., Lagakos, W.S., Talukdar, S., Osborn, O., Johnson, A., Chung, H., Maris, M., Ofrecio, J.M., et al. (2015). LTB4 promotes insulin resistance in obese mice by acting on macrophages, hepatocytes and myocytes. Nat. Med. *21*, 239–247.

Li, P., Liu, S., Lu, M., Bandyopadhyay, G., Oh, D., Imamura, T., Johnson, A.M., Sears, D., Shen, Z., Cui, B., et al. (2016). Hematopoietic-derived galectin-3 causes cellular and systemic insulin resistance. Cell *167*, 973–984.e912.

Lo, J., Bernstein, L.E., Canavan, B., Torriani, M., Jackson, M.B., Ahima, R.S., and Grinspoon, S.K. (2007). Effects of TNF-alpha neutralization on adipocytokines and skeletal muscle adiposity in the metabolic syndrome. Am. J. Physiol. Endocrinol. Metab. *293*, E102–E109.

Lumeng, C.N., Deyoung, S.M., Bodzin, J.L., and Saltiel, A.R. (2007). Increased inflammatory properties of adipose tissue macrophages recruited during diet-induced obesity. Diabetes *56*, 16–23.

Lumeng, C.N., DelProposto, J.B., Westcott, D.J., and Saltiel, A.R. (2008). Phenotypic switching of adipose tissue macrophages with obesity is generated by spatiotemporal differences in macrophage subtypes. Diabetes *57*, 3239–3246.

Mallory, A.C., Reinhart, B.J., Jones-Rhoades, M.W., Tang, G., Zamore, P.D., Barton, M.K., and Bartel, D.P. (2004). MicroRNA control of PHABULOSA in leaf development: importance of pairing to the microRNA 5′ region. EMBO J. *23*, 3356–3364.

Morinaga, H., Mayoral, R., Heinrichsdorff, J., Osborn, O., Franck, N., Hah, N., Walenta, E., Bandyopadhyay, G., Pessentheiner, A.R., Chi, T.J., et al. (2015). Characterization of distinct subpopulations of hepatic macrophages in HFD/obese mice. Diabetes *64*, 1120–1130.

Nguyen, M.T.A., Favelyukis, S., Nguyen, A.K., Reichart, D., Scott, P.A., Jenn, A., Liu-Bryan, R., Glass, C.K., Neels, J.G., and Olefsky, J.M. (2007). A subpopulation of macrophages infiltrates hypertrophic adipose tissue and is activated by free fatty acids via Toll-like receptors 2 and 4 and JNK-dependent pathways. J. Biol. Chem. *282*, 35279–35292.

Ofei, F., Hurel, S., Newkirk, J., Sopwith, M., and Taylor, R. (1996). Effects of an engineered human anti-TNF-alpha antibody (CDP571) on insulin sensitivity and glycemic control in patients with NIDDM. Diabetes *45*, 881–885.

Ogden, C.L., Carroll, M.D., Lawman, H.G., Fryar, C.D., Kruszon-Moran, D., Kit, B.K., and Flegal, K.M. (2016). Trends in obesity prevalence among children and adolescents in the United States, 1988-1994 Through 2013-2014. JAMA *315*, 2292–2299.

Oh, D.Y., Morinaga, H., Talukdar, S., Bae, E.J., and Olefsky, J.M. (2012). Increased macrophage migration into adipose tissue in obese mice. Diabetes *61*, 346–354.

Ortega, F.J., Mercader, J.M., Moreno-Navarrete, J.M., Rovira, O., Guerra, E., Esteve, E., Xifra, G., Martínez, C., Ricart, W., Rieusset, J., et al. (2014). Profiling of circulating microRNAs reveals common microRNAs linked to type 2 diabetes that change with insulin sensitization. Diabetes Care *37*, 1375–1383.

Ortega, F.J., Moreno, M., Mercader, J.M., Moreno-Navarrete, J.M., Fuentes-Batllevell, N., Sabater, M., Ricart, W., and Fernández-Real, J.M. (2015). Inflammation triggers specific microRNA profiles in human adipocytes and macrophages and in their supernatants. Clin. Epigenetics *7*, 49.

Paquot, N., Castillo, M.J., Lefèbvre, P.J., and Scheen, A.J. (2000). No increased insulin sensitivity after a single intravenous administration of a recombinant human tumor necrosis factor receptor: Fc fusion protein in obese insulin-resistant patients. J. Clin. Endocrinol. Metab. *85*, 1316–1319.

Pescador, N., Pérez-Barba, M., Ibarra, J.M., Corbatón, A., Martínez-Larrad, M.T., and Serrano-Ríos, M. (2013). Serum circulating microRNA profiling for identification of potential type 2 diabetes and obesity biomarkers. PLoS ONE *8*, e77251.

Romeo, G.R., Lee, J., and Shoelson, S.E. (2012). Metabolic syndrome, insulin resistance, and roles of inflammation–mechanisms and therapeutic targets. Arterioscler. Thromb. Vasc. Biol. *32*, 1771–1776.

Shi, Z., Zhao, C., Guo, X., Ding, H., Cui, Y., Shen, R., and Liu, J. (2014). Differential expression of microRNAs in omental adipose tissue from gestational diabetes mellitus subjects reveals miR-222 as a regulator of ERα expression in estrogen-induced insulin resistance. Endocrinology *155*, 1982–1990.

Shoelson, S.E., Lee, J., and Yuan, M. (2003). Inflammation and the IKK beta/I kappa B/NF-kappa B axis in obesity- and diet-induced insulin resistance. Int. J. Obes. Relat. Metab. Disord. *27* (*Suppl 3*), S49–S52.

Spite, M., Hellmann, J., Tang, Y., Mathis, S.P., Kosuri, M., Bhatnagar, A., Jala, V.R., and Haribabu, B. (2011). Deficiency of the leukotriene B4 receptor, BLT-1, protects against systemic insulin resistance in diet-induced obesity. J. Immunol. *187*, 1942–1949.

Sugii, S., Olson, P., Sears, D.D., Saberi, M., Atkins, A.R., Barish, G.D., Hong, S.H., Castro, G.L., Yin, Y.Q., Nelson, M.C., et al. (2009). PPARgamma activation in adipocytes is sufficient for systemic insulin sensitization. Proc. Natl. Acad. Sci. USA *106*, 22504–22509.

Thai, T.H., Calado, D.P., Casola, S., Ansel, K.M., Xiao, C., Xue, Y., Murphy, A., Frendewey, D., Valenzuela, D., Kutok, J.L., et al. (2007). Regulation of the germinal center response by microRNA-155. Science *316*, 604–608.

Thomou, T., Mori, M.A., Dreyfuss, J.M., Konishi, M., Sakaguchi, M., Wolfrum, C., Rao, T.N., Winnay, J.N., Garcia-Martin, R., Grinspoon, S.K., et al. (2017). Adipose-derived circulating miRNAs regulate gene expression in other tissues. Nature *542*, 450–455.

Toda, A., Yokomizo, T., and Shimizu, T. (2002). Leukotriene B4 receptors. Prostaglandins Other Lipid Mediat. *68-69*, 575–585.

Tontonoz, P., and Spiegelman, B.M. (2008). Fat and beyond: the diverse biology of PPARgamma. Annu. Rev. Biochem. *77*, 289–312.

Tontonoz, P., Hu, E., and Spiegelman, B.M. (1994). Stimulation of adipogenesis in fibroblasts by PPAR gamma 2, a lipid-activated transcription factor. Cell *79*, 1147–1156.

Trajkovic, K., Hsu, C., Chiantia, S., Rajendran, L., Wenzel, D., Wieland, F., Schwille, P., Brügger, B., and Simons, M. (2008). Ceramide triggers budding of exosome vesicles into multivesicular endosomes. Science *319*, 1244–1247.

Valadi, H., Ekström, K., Bossios, A., Sjöstrand, M., Lee, J.J., and Lötvall, J.O. (2007). Exosome-mediated transfer of mRNAs and microRNAs is a novel mechanism of genetic exchange between cells. Nat. Cell Biol. *9*, 654–659.

Weisberg, S.P., McCann, D., Desai, M., Rosenbaum, M., Leibel, R.L., and Ferrante, A.W., Jr. (2003). Obesity is associated with macrophage accumulation in adipose tissue. J. Clin. Invest. *112*, 1796–1808.

Xu, H., Barnes, G.T., Yang, Q., Tan, G., Yang, D., Chou, C.J., Sole, J., Nichols, A., Ross, J.S., Tartaglia, L.A., and Chen, H. (2003). Chronic inflammation in fat plays a crucial role in the development of obesity-related insulin resistance. J. Clin. Invest. *112*, 1821–1830.

Ying, W., Cheruku, P.S., Bazer, F.W., Safe, S.H., and Zhou, B. (2013). Investigation of macrophage polarization using bone marrow derived macrophages. J. Vis. Exp. *76*, e50323.

Yuyama, K., Sun, H., Mitsutake, S., and Igarashi, Y. (2012). Sphingolipid-modulated exosome secretion promotes clearance of amyloid-β by microglia. J. Biol. Chem. *287*, 10977–10989.

Zampetaki, A., Kiechl, S., Drozdov, I., Willeit, P., Mayr, U., Prokopi, M., Mayr, A., Weger, S., Oberhollenzer, F., Bonora, E., et al. (2010). Plasma microRNA profiling reveals loss of endothelial miR-126 and other microRNAs in type 2 diabetes. Circ. Res. *107*, 810–817.

Zhang, J., Li, S., Li, L., Li, M., Guo, C., Yao, J., and Mi, S. (2015a). Exosome and exosomal microRNA: trafficking, sorting, and function. Genomics Proteomics Bioinformatics *13*, 17–24.

Zhang, L., Zhang, S., Yao, J., Lowery, F.J., Zhang, Q., Huang, W.C., Li, P., Li, M., Wang, X., Zhang, C., et al. (2015b). Microenvironment-induced PTEN loss by exosomal microRNA primes brain metastasis outgrowth. Nature *527*, 100–104.

Zhang, Y., Shi, L., Mei, H., Zhang, J., Zhu, Y., Han, X., and Zhu, D. (2015c). Inflamed macrophage microvesicles induce insulin resistance in human adipocytes. Nutr. Metab. (Lond.) *12*, 21–34.

# STAR★METHODS

## KEY RESOURCES TABLE

| REAGENT or RESOURCE | SOURCE | IDENTIFIER |
|---|---|---|
| Antibodies | | |
| Rabbit polyclonal anti-HSP90 | Santa Cruz | Cat# sc-382636 |
| Mouse monoclonal anti-PPARγ | Santa Cruz | Cat# sc-7273; RRID:AB_628115 |
| Mouse monoclonal anti-HSP70 | Santa Cruz | Cat# sc-24; RRID:AB_627760 |
| Rabbit monoclonal anti-phospho-Akt (Ser473) | Cell Signaling Technology | Cat# 9271; RRID:AB_329825 |
| Mouse monoclonal anti-Akt (pan) | Cell Signaling Technology | Cat# 2920; RRID:AB_1147620 |
| Rabbit monoclonal anti-GAPDH | Cell Signaling Technology | Cat# 5174; RRID:AB_10622025 |
| Rabbit monoclonal anti-Phospho-NF-κB p65 | Cell Signaling Technology | Cat# 3033; RRID:AB_331284 |
| Rabbit monoclonal anti-NF-κB p65 | Cell Signaling Technology | Cat# 8242; RRID:AB_10859369 |
| Rabbit monoclonal anti-Drosha | Cell Signaling Technology | Cat# 3364; RRID:AB_2238644 |
| Rabbit polyclonal anti-GLUT4 | EMD Millipore | Cat# 07-1404 |
| Rabbit polyclonal anti-CD63 | Abcam | Cat# ab68418; RRID:AB_10563972 |
| Rabbit monoclonal anti-CD9 | Abcam | Cat# ab92726; RID:AB_10561589 |
| Rabbit monoclonal anti-TSG101 | Abcam | Cat# ab125011; RRID:AB_10974262 |
| Rabbit polyclonal anti-Syntenin 1 | ThermoFisher Scientific | Cat# PA5-28826; RRID:AB_2546302 |
| PE-Cyanine7 anti-mouse F4/80 angtigen | eBioscience | Cat# 25-4801-82; RRID:AB_469653 |
| Alexa Fluor 488 anti-mouse CD11b | eBioscience | Cat# 53-0112-82; RRID:AB_469901 |
| APC anti-mouse CD11c | eBioscience | Cat# 17-0114-82; RRID:AB_469346 |
| PE anti-mouse CD206 | Biolegend | Cat# 141706; RRID:AB_10895754 |
| PE-Cyanine7 anti-mouse CD45 | eBioscience | Cat# 25-0451-82; RRID:AB_469625 |
| Chemicals, Peptides, and Recombinant Proteins | | |
| Novolin R regular human insulin in ITTs | Novo-Nordisk | Cat# NDC 0169-1833-11 |
| Insulin used in glucose uptake and hepatic glucose production assays | Sigma-Aldrich | Cat# I9278 |
| Liberase TM Research Grade | Roche | Cat# 05401119001 |
| 2-deoxy-D-glucose | Sigma-Aldrich | Cat# D8375 |
| Dextrose | Hospira, Inc | Cat# 0409-6648-02 |
| $^{14}$C-pyruvate | Perkin Elmer | Cat# NEC256050UC |
| $^{3}$H-deoxyglucose | Perkin Elmer | Cat# NET328001MC |
| $^{3}$H-glucose | Perkin Elmer | Cat# NET331C001MC |
| PKH26 | Sigma-Aldrich | Cat# PKH26GL-1KT |
| GW4869 (hydrochloride hydrate) | Cayman Chemical | Cat# 6823-69-4 |
| 60% high fat diet | Research Diets | Cat# D12492 |
| AG-501X8 Resin | Bio-Rad Laboratories | Cat# 143-7424 |
| Liposome control | FormuMax | Cat# F70101-N |
| Exosome-depleted FBS | SBI | Cat# EXO-FBSHI-50A-1 |
| Lipofectamine RNAiMAX reagent | Thermo Fisher Scientific | Cat# 13778-075 |
| Collagenase II | Sigma-Aldrich | Cat# C2674 |
| OptiPrep density gradient medium | Sigma-Aldrich | Cat# D1556-250ML |
| Rosiglitazone | Sigma-Aldrich | Cat# R2408-10MG |
| Percoll | GE Healthcare Life Sciences | Cat# 17-0891-01 |
| TRIzol RNA isolation reagent | Thermo Fisher Scientific | Cat# 15596026 |
| SuperSignal West Pico Chemiluminescent Substrate | Thermo Fisher Scientific | Cat# 34077 |

(*Continued on next page*)

*Continued*

| REAGENT or RESOURCE | SOURCE | IDENTIFIER |
|---|---|---|
| Halt Protease and Phosphatase Inhibitor Cocktail | Thermo Fisher Scientific | Cat# 78440 |
| RIPA buffer (10x) | Cell Signaling Technology | Cat# 9806 |
| Critical Commercial Assays | | |
| RNA purification kit | Zymo research | Cat# R2060 |
| Plasma FFA enzymatical kit | WAKO Chemicals | Cat# 999-34691 |
| Mouse FGF21 ELISA kit | Abcam | Cat# ab212160 |
| miRCURY RNA isolation kit-Biofluids | EXIQON | Cat# 300112 |
| miRNA Target IP Kit | ACTIVE MOTIF | Cat# 25500 |
| Insulin ELISA kit | ALPCO | Cat# 80-INSHU-E01.1 |
| Deposited Data | | |
| Small RNA seq raw data | NIH GEO database | GSE97652 |
| EV TRACK knowledgebase | http://evtrack.org/review.php | GH3543TZ |
| Experimental Models: Cell Lines | | |
| 3T3-L1 adipocyte | ATCC | N/A |
| L6 skeletal myoblast | Amira Klip's laboratory | N/A |
| Primary hepatocyte | This paper | N/A |
| Bone marrow-derived macrophage | This paper | N/A |
| Experimental Models: Organisms/Strains | | |
| Mouse: WT C57BL6/J | Jackson Laboratories | JAX:000664 |
| Mouse: miR-155$^{tm1.Rsky}$/J | Jackson Laboratories | JAX: 007745 |
| Mouse: C57BL6-Tg(CAG-EGFP) | Jackson Laboratories | JAX:003291 |
| Oligonucleotides | | |
| miR-223 RT-PCR primer (Stem-loop sequence: UCUGGCCAUCUGCAGUGUCACGCUCCGUGUAUUU GACAAGCUGAGUUGGACACUCUGUGUGGUAGAG UGUCAGUUUGUCA AAUACCCCAAGUGUGGCUCAUGCCUAUCAG) | Thermo Fisher Scientific | Assay ID 007896_mat |
| miR-155 RT-PCR primer (Stem-loop sequence: CUGUUAAUGCUAAUUGUGAUAGGGGUUUU GGCCUCUGACUGACUCCUACCUGUUAGCAUUAACAG) | Thermo Fisher Scientific | Assay ID 002571 |
| U6 snRNA RT-PCR primer | Thermo Fisher Scientific | Cat# 4427975 |
| miR-155 mimic | Thermo Fisher Scientific | Cat# 4464066 |
| Cy3-labeled miR-223 mimic | GE Dharmacon | Cat# SO-2465930G |
| Silencer siRNA-Drosha | Thermo Fisher Scientific | Cat# AM16708 |
| miRNA mimic negative control | Thermo Fisher Scientific | Cat# 4464058 |
| Silencer negative control siRNA | Thermo Fisher Scientific | Cat# AM4611 |
| Software and Algorithms | | |
| FlowJo | FlowJo | https://www.flowjo.com/ |
| Image Lab | BioRad | http://www.bio-rad.com/en-us/product/image-lab-software |
| ChemiDoc XRS imaging system | BioRad | http://www.bio-rad.com/en-us/product/chemidoc-imaging-systems/chemidoc-xrs-system |
| Prism | Graphpad | https://www.graphpad.com/scientific-software/prism/ |

## CONTACT FOR REAGENT AND RESOURCE SHARING

Further information and requests for reagents may be directed to Lead Contact, Jerrold M. Olefsky (jolefsky@ucsd.edu).

## EXPERIMENTAL MODEL AND SUBJECT DETAILS

### Animal care and use

The generation of miR-155KO mice has been previously described (Thai et al., 2007). Wild-type (WT) C57BL6 and GFP-WT mice were received from the Jackson Laboratory. All mice were maintained on a 12/12 hr light-dark cycle. Male mice 8 weeks of age were fed ad libitum. Mice were fed a high-fat diet (60% fat calories, 20% protein calories, and 20% carbohydrate calories; Research Diets) or a normal chow diet.

### *Cell lines and primary hepatocytes*

To generate adipocytes, 3T3-L1 cells were differentiated in the induction medium (DMEM/F12 medium containing 10% FBS, penicillin-streptomycin, and glutamine and then induced with a differentiation cocktail consisting of 0.5 mM 3-isobutyl-1-methylxanthine, 1 μM dexamethasone, 10 μg/mL insulin, 0.2 mM indomethacin, and 1 μM rosiglitazone in DMEM supplemented with 10% FBS, PS, and glutamine) for 7-10 days. To induce myotube formation, L6 skeletal myoblasts were cultured in MEM medium with 4% FBS for 8-10 days (Li et al., 2016).

Primary hepatocytes were isolated as described previously (Li et al., 2016). Briefly, mice were infused with a calcium free HEPES-phosphate buffer A (Calcium and magnesium-free PBS containing 0.2 uM EGTA, 10 mM HEPES, 1 mM glucose and 0.2% BSA, pH 7.4) via the vena cava for 3-5 min. After the color of the liver changed to a beige or light brown color, collagenase-containing buffer B (PBS with 1 mM magnesium and 1 mM calcium, 0.2% BSA, and 30 mM HEPES, 40 μg collagenase/ml (Liberase TM, Roche) was perfused into liver for 2-3 min. After the appearance of cracking on the surface of liver, perfusion was stopped immediately and the liver was excised into ice-cold buffer A. Cells from digested livers were teased out, suspended in Buffer A, filtered through 100 μm nylon filter, and centrifuged at 60 x g for 6 min at 4°C. The pellet was washed with Buffer B (no collagenase) twice and then mixed with Percoll (adjusted to physiological ionic strength with 10x PBS) to a final concentration of 36% and centrifuged at 100 x g for 10 min, 4°C. After removing the supernatant, the hepatocyte pellet was washed once with Buffer B (without collagenase) and then cultured in Williams Medium E (Life Technologies) containing 10 nM dexamethasone and 10% FBS on collagen-coated plates (GIBCO, Life Technologies) and antibiotics. After overnight incubation (16 hr), culture medium was switched to a serum-free Williams E medium containing 0.2% BSA and antibiotics. The macrophage contamination in isolated primary hepatocytes was examined by measuring the expression of myeloid cell-specific genes *Emr1* and miR-223 and cell surface markers CD11b and F4/80.

## METHODS DETAILS

### Glucose tolerance and insulin tolerance tests and hyperinsulinemic-euglycemic clamp studies

For glucose tolerance tests, mice received one dose of dextrose (1 g/kg body weight) via i.p. injection after 12 hr of fasting. For insulin tolerance tests, mice were fasted for 6 hr and then i.p. injected with insulin (0.70 units/kg body weight).

To perform hyperinsulinemic-euglycemic clamp assays, dual catheters (MRE-025, Braintree Scientific) were implanted in the right jugular vein and tunneled subcutaneously and exteriorized at the back of the neck. Three to five days after recovery, 6 hr fasted mice were infused with D-[3-3H] glucose (Perkin Elmer) for 90 min. After tracer equilibration, blood sampling occurred, then glucose (50% dextrose) and tracer (5 μCi/h) plus insulin (8 mU/kg/min) were infused into the jugular vein. Blood samples were measured from the tail vein at 10 min intervals. The steady-state conditions (120 mg/dl ± 10 mg/dl) was confirmed at the end of the clamp by maintaining glucose infusion and plasma glucose concentration for a minimum of 20 min. Blood samples at time point = −10, 0 (basal), 110, and 120 (end of experiment) min were collected to determine glucose-specific activity, as well as free fatty acid and insulin concentration. Tracer-determined rates were quantified by using the Steele equation for steady-state conditions. At steady state, the rate of glucose disappearance (GDR) is equal to the sum of the rate of endogenous glucose productions (HGP) plus the exogenous GIR. The IS-GDR is equal to the total GDR minus the basal glucose turnover rate.

### In vivo insulin-stimulated AKT phosphorylation assay

Tissue insulin action was evaluated by measuring insulin-stimulated AKT phosphorylation in liver, skeletal muscle, and VAT. Briefly, after 8 hr fasting, mice were anesthetized and parts of these insulin target tissues were collected to measure basal level of AKT phosphorylation. After a dose of insulin (0.75 U/kg body weight) injected via vena cava, parts of liver, skeletal muscle, and VAT were collected at 3 min, 7 min, and 10 min, respectively. The phosphorylation of ATK was measured by western blot analysis with antibodies against phosphorylated ATK (s473) or pan-AKT.

### Isolation of stromal cells from visceral adipose tissue

Visceral adipose tissues (VATs) were mechanically chopped and then digested with collagenase II (Sigma-Aldrich) for 15 min at 37°C. After passing cells through a 100 μm cell strainer and centrifugation at 1,000 x g for 10 min, primary adipocytes were collected from the top layer of the supernatant and the pellet containing the stromal vascular cell (SVC) fraction was then incubated with red blood cell lysis buffer. The macrophage contamination in isolated primary adipocytes was examined by measuring the expression of myeloid cell-specific genes *Emr1* and miR-223 and cell surface markers CD11b and F4/80.

### Adipose tissue macrophage isolation

Adipose tissue macrophages (ATMs) were isolated from VAT of NCD and HFD WT mice. SVC single cell suspensions were incubated with fluorescence-tagged antibodies against CD11b or F4/80. CD11b+F4/80+ macrophages were purified using BD FACS Aria II flow cytometer (BD Biosciences). ATMs were then cultured in IMDM containing 10% exosome-free FBS to produce exosomes.

### Primary pre-adipocyte isolation and adipocyte differentiation

Subcutaneous pre-adipocytes derived from stromal vascular cells were obtained by collagenase digestion. In detail, subcutaneous fat tissue from NCD miR-155KO mice was dissected and minced. The minced tissues were digested with 2 mg/mL collagenase II (Sigma-Aldrich) in Hank's buffered salt solution (HBSS) containing 10 mM HEPES and 0.1% bovine serum albumin in a water bath with shaking at 37°C for 30 min. The digested tissues were filtered through a 100 μm filter and centrifuged at 50 g for 5 min to remove the floating cell layer. The stromal vascular cells were pelleted by centrifugation at 500 x g for 5 min and incubated in red blood cell lysis buffer for 5 min at room temperature. Finally, subcutaneous pre-adipocytes were isolated through filtration with a 40 μm filter and centrifugation at 500 x g for 5 min.

For adipocyte differentiation, pre-adipocytes were first cultured to confluence in DMEM/F12 medium containing 10% FBS, penicillin-streptomycin (PS), and glutamine and then induced with a differentiation cocktail consisting of 0.5 mM 3-isobutyl-1-methylxanthine, 1 μM dexamethasone, 10 μg/mL insulin, 0.2 mM indomethacin, and 1 μM rosiglitazone in DMEM supplemented with 10% FBS, PS, and glutamine. After 3 days, the medium was replaced to DMEM containing 10% FBS, penicillin streptomycin, glutamine, 10 μg/mL insulin, and 1 μM rosiglitazone every other day.

#### *Differentiation and activation of bone marrow-derived macrophages*

Bone marrow-derived macrophages (BMDMs) were prepared as previously described (Ying et al., 2013). BMDMs were stimulated with LPS (100 ng/ml) for M1 polarized activation.

### Exosome purification and characterization

After 72 hr ATM culture, debris and dead cells in the medium were removed by centrifugation at 1000 x g for 10 min and then filtrated through 0.2 μm filter. The medium was then subjected to ultracentrifugation at 100,000 x g for 4∼6 hr at 4°C. After wash with PBS (100,000 x g for 20 min), the exosome-containing pellet was resuspended in PBS. The characterization of exosomes was confirmed by measuring expression of exosome-specific markers TSG101 and Syntenin 1, and EV-associated protein markers HSP70, CD63, and CD9 by western blot analysis and particle size by NanoSight analysis (Malvern Instruments). In addition, we further examined the characteristics of EVs using iodixanol gradient centrifugation as reported by Kowal et al. (2016). The information about exosome preparation is uploaded to the EV-TRACK knowledgebase. Readers may access the experimental parameters in the EV-TRACK knowledgebase in the following URL: http://evtrack.org/review.php. The EV-TRACK code is GH3543TZ. To monitor exosome trafficking, exosomes were labeled with PKH26 fluorescent dye using the PKH26 fluorescent cell linker kit (Sigma-Aldrich). After PKH26 staining, the exosomes were washed in PBS and collected by ultracentrifugation (100,000 x g for 20 min) at 4°C. Finally PKH26-labeled exosomes were resuspended in PBS.

### Electron microscopy

For electron microscopy, exosomes were fixed with 2% paraformaldehyde and loaded on Formvar and carbon-coated copper grids. Then the grids were placed on 2% gelatin at 37°C for 20 min, rinsed with 0.15 M glycine/PBS and the sections were blocked using 1% cold water fish-skin gelatin. Grids were viewed using a JEOL 1200EX II (JEOL) transmission electron microscope and photographed using a Gatan digital camera (Gatan).

### In vivo and in vitro exosome treatment

For *in vitro* treatment, 2 μg of exosomes on the basis of protein measurement were added to $1 \times 10^5$ recipient cells. Previous study has shown that the quantity of circulating exosomes in obese mice is approximately 30 μg/mouse (Deng et al., 2009). Therefore, for *in vivo* treatment, ATM-derived exosomes (30 μg every 7 days) were adoptively transferred into recipient mice via tail vein injection. In the control groups, empty liposome (FormuMax) was used.

### miRNA mimic or siRNA transfection

Cy3 labeled miRNA mimic (GE Dharmacon) or siRNA-Drosha (ThermoFisher Scientific) was transfected into recipient cells with the lipofectamine RNAiMAX reagent (ThermoFisher Scientific). After 24 hr, the transfection efficiencies were validated by either qPCR or western blot analysis.

### Argonaut-RNA co-immunoprecipitation assay

After miR-155 overexpression in 3T3 adipocytes, L6 myocytes, or primary hepatocytes, the argonaut protein immunoprecipitation and purification of total RNAs associated with argonaut were performed with the miRNA Target IP Kit (Active Motif).

### Co-culture assay

After transfection with Cy3-miR-223 mimic, BMDMs ($0.1 \times 10^6$/well) were co-cultured with 3T3 adipocytes at a ratio of 1:1 using a trans-well plate (0.4 μm polycarbonate filter, Corning) for 12 hr, with 3T3 adipocytes placed in the lower chamber and BMDM cells in the upper chamber. The BMDMs treated with Cy3 dye only (without miRNA mimic) were used in the control group. After washing with PBS twice, the appearance of Cy3 red fluorescence on 3T3 adipocytes was examined. To inhibit EV secretion, ATMs were pretreated with GW4869 (an inhibitor of neutral sphingomyelinase, 10 μM) (Trajkovic et al., 2008; Yuyama et al., 2012) for 24 hr. These ATMs were used to co-culture with 3T3-L1 adipocytes in the medium containing GW4869 for another 12 hr.

### Flow cytometry analysis

Unless otherwise specified, we purchased antibodies from eBioscience. Visceral stromal cells were stained with fluorescence-tagged antibodies to detect cell lineages. Macrophage subtypes were detected with antibodies against F4/80, Cd11b, Cd206 (Cat. No. 141706, Biolegend), Cd11c (Cat. No. 12-0114-83). Data were analyzed using Flowjo software.

### Glucose uptake assay

After 8 hr serum starvation, cells were stimulated with 100 nM insulin for 30 min in KRH buffer (137 nM NaCl, 4.8 mM KCl, 1.2 mM $KH_2PO_4$, 1.2 mM $MgSO_4$, 2.5 mM $CaCl_2$, 0.2% BSA, 16 mM HEPES) at 37°C. Then 3H-2-deoxy-D-glucose (3H-2-DOG, 0.1 mM, 0.4 μCi/ml) was supplemented to cells. After 10 min incubation at 37°C, cells were washed with ice-cold PBS twice. NaOH (1 N) was then added and incubated for 20 min to efficiently dissolve cells. An aliquot was used for protein concentration measurement. After neutralizing NaOH by adding HCl (1 N), the extracts were transferred to scintillation vials, and scintillation fluid was added and the radioactivity was counted. Results were normalized with protein concentration of cell lysates.

### Glucose output assay

After exosome treatment or miR-155 overexpression, primary hepatocytes were exposed to glucose-free buffer containing glucagon (100 ng/ml), insulin (10 nM), or a combination of glucagon and insulin for 30 min, at 37°C. Then 2-$^{14}$C-pyruvate (2 mM, final) was added to cells as substrate to initiate gluconeogenesis and incubated for 2.5 hr. Culture media were collected in tubes and deproteinized by adding $Ba(OH)_2$ (0.3 N) and 5% $ZnSO_4$. The mixture was vortexed and centrifuged at 10,000 x g for 5 min. One ml of supernatant from each tube was vortexed with mixed anion and cation exchange resins (BioRad) and then centrifuged at 10,000 x g, 5 min. Half of 1 mL of each supernatant was transferred to a scintillation vial for radioactivity measurement. The supernatants were counted as free $^{14}$C-glucose. The primary hepatocytes attached the culture plate were dissolved by adding NaOH (1 N) and protein content was determined. The radioactivity results were normalized by total protein to obtain radioactivity per mg protein.

### Western blot analysis

Cells or tissues were homogenized in RIPA buffer supplemented with protease and phosphatase inhibitors (ThermoFisher Scientific). Equal amounts of cell lysate proteins from each biological replicate were subjected to western blotting. Using ChemiDoc XRS imaging system (BioRad), the protein bands on blots were detected with the SuperSignal West Pico Chemiluminescent Substrate (Thermo Scientific). The exposure time to detect PPARγ and GLUT4 protein bands is included in figure legends. Protein bands were analyzed using Image Lab software (BioRad). Arbitrary densitometry units were quantified and were expressed as mean ± SEM. We normalized phosphorylated protein to total protein bands, or normalized protein expression to housekeeping protein bands. Western blot data in figures and supplemental figures are all representative of more than three independent experiments.

### RNA extraction and miRNA RT-qPCR assay

Total RNAs were extracted from cells using the Direct-zol RNA MicroPrep kit (Zymo research). The exosomal RNAs were extracted by the miRCURY RNA isolation kit-Biofluids (EXIQON). The cellular or exosomal miRNA expression was measured as previously described (Fong et al., 2015). Data were normalized to levels of U6 (cellular) or total protein of exosomes.

#### *Small RNA deep sequencing and bioinformatics analysis*

miRNA components in either lean ATM-Exos (n = 7) or obese ATM-Exos were profiled by the small RNA sequencing analysis (Illumina). miRNA-seq reads were quality-assessed with FastQC and MultiQC, then trimmed with Trimmomatic 0.30 and subsequently aligned with NovoAlign to all mouse miRNA hairpin sequences in release 21 of miRBase. The resulting alignments were tabulated with a python script to generate per-miRNA counts. Using a custom analysis pipeline developed in an R-kernel Jupyter Notebook, very low expressed miRNAs and those not represented in at least ~1/3 of samples were filtered, and the remaining data were subjected to TMM (trimmed mean of M values) normalization using the EdgeR package in Bioconductor. Principal component analysis demonstrated that negligible library-size or batch effects remained. The voom method was used in conjunction with the limma package to estimate precision weights for all observations and then identify differentially expressed miRNAs. Visualizations were generated with the ggplot2, Venn Diagram and heatmap3 R packages. Sequencing data supporting these studies can be found at the Gene Expression Omnibus database under accession number GSE97652.

### Bone marrow transplantation

To generate irradiated chimeras, 10 week old miR-155KO recipient mice received a lethal dose of 10 Gy radiation, followed by tail-vein injection of $2 \times 10^6$ bone marrow cells from either GFP-WT or miR-155KO mice. After 4 weeks, engraftment of WT donor cells was examined by the present of GFP+CD45+ cells in peripheral blood. After 8 weeks of bone marrow transplantation (BMT), all mice were subjected to a HFD feeding regimen for an additional 20 weeks.

## QUANTIFICATION AND STATISTICAL ANALYSIS

Results are expressed as mean ± SEM. Each data point derived from qPCR assays represents an average of at least two technical replicates. The statistical significance of the differences between various treatments was measured by either the two tailed Student's t test or one-way ANOVA with Bonferroni post-test. Data analyses were performed using GraphPad Prism software version 6.0. A value of $p < 0.05$ was considered statistically significant.

### Study approval

All animal procedures were done in accordance with University of California, San Diego Research Guidelines for the Care and Use of Laboratory Animals and all animals were randomly assigned to cohorts when used.

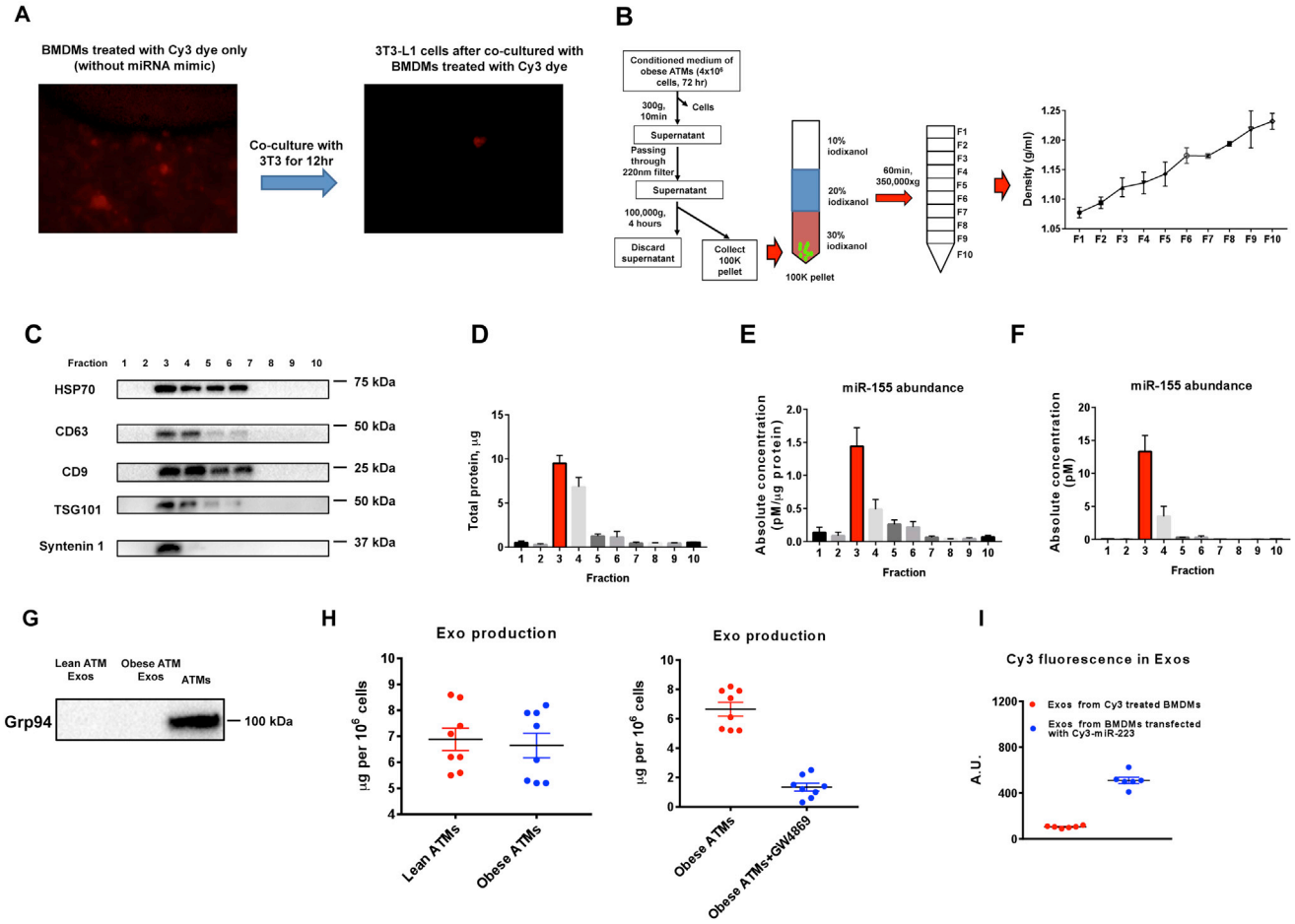


**Figure S1. Characteristics of Macrophage-Derived Exos, Related to Figure 1**

(A) In the control group, the appearance of Cy3 red fluorescence on 3T3-L1 adipocytes was examined after co-culture with M0 bone marrow-derived macrophages (BMDMs) treated with Cy3 dye (without miR-223 mimic) for 12 hr. (B) Iodixanol gradient floatation separation of EVs derived from obese ATM into 10 subfractions. (C–F) exosome-specific markers and miR-155 abundance in subfractions after iodixanol gradient floatation. (G) The endoplasmic reticulum protein Grp94 was not detected in either lean or obese adipose tissue macrophage (ATM)-derived Exos. This blot is representative of 3 replicate independent experiments. (H) Exosome production by macrophages. (I) Cy3 fluorescence intensity was measured in Exos collected from BMDM control (Cy3 dye treated) and BMDMs transfected with Cy3-miR-223. In the western blot analyses, each well was loaded with 10 μg protein. These blots are representative of 3 replicated independent experiments. Data are presented as mean ± SEM. (H), n = 8 per group. (I), n = 6 per group.

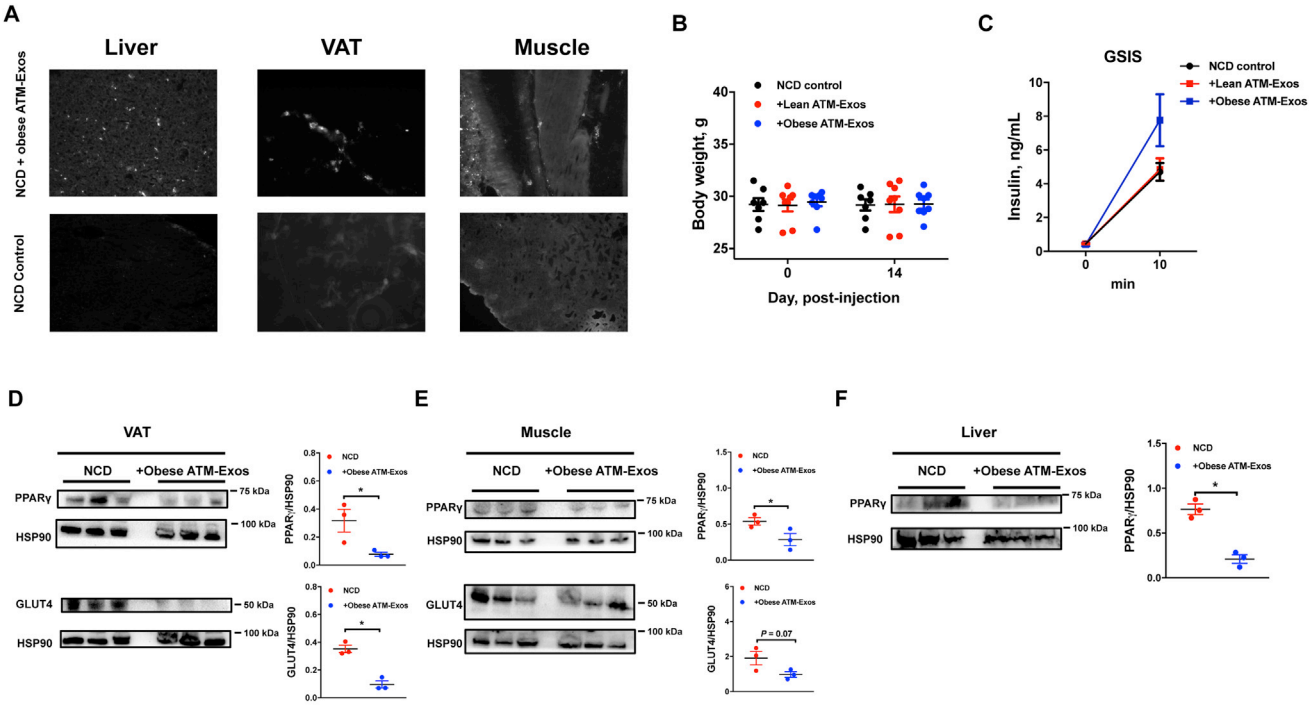


**Figure S2. Effects of Obese ATM-Exos on Metabolism in NCD Recipient Mice, Related to Figure 2**

(A) Appearance of PKH26-labeled Exos in liver, visceral adipose tissue (VAT), and muscle of WT NCD recipient mice after 16 hr administration of obese ATM exosomes (ATM-Exos). Representative images are shown from 3 independent experiments. NCD, normal chow diet. (B and C) Body weight (B) and glucose-stimulated insulin secretion (GSIS, (C) in NCD WT recipient mice treated with ATM-Exos. (D–F) Expression of PPARγ in VAT (D), muscle (E), and liver (F) of NCD WT mice after treatment with obese ATM-Exo for 2 weeks. In the western blot analyses, the exposure time to detect PPARγ in VAT (D), muscle (E), and liver tissue (F) was 80 s (s), 580 s, and 600 s, respectively. The exposure time to detect GLUT4 in VAT and muscle was 120 s and 80 s, respectively. These blots are representative of 3 replicated independent experiments. Data are presented as mean ± SEM. (B) and (C), n = 7 for NCD control group, and n = 8 for the other groups. (C), NCD control versus +Obese ATM-Exos, p = 0.062 by Student's t test.

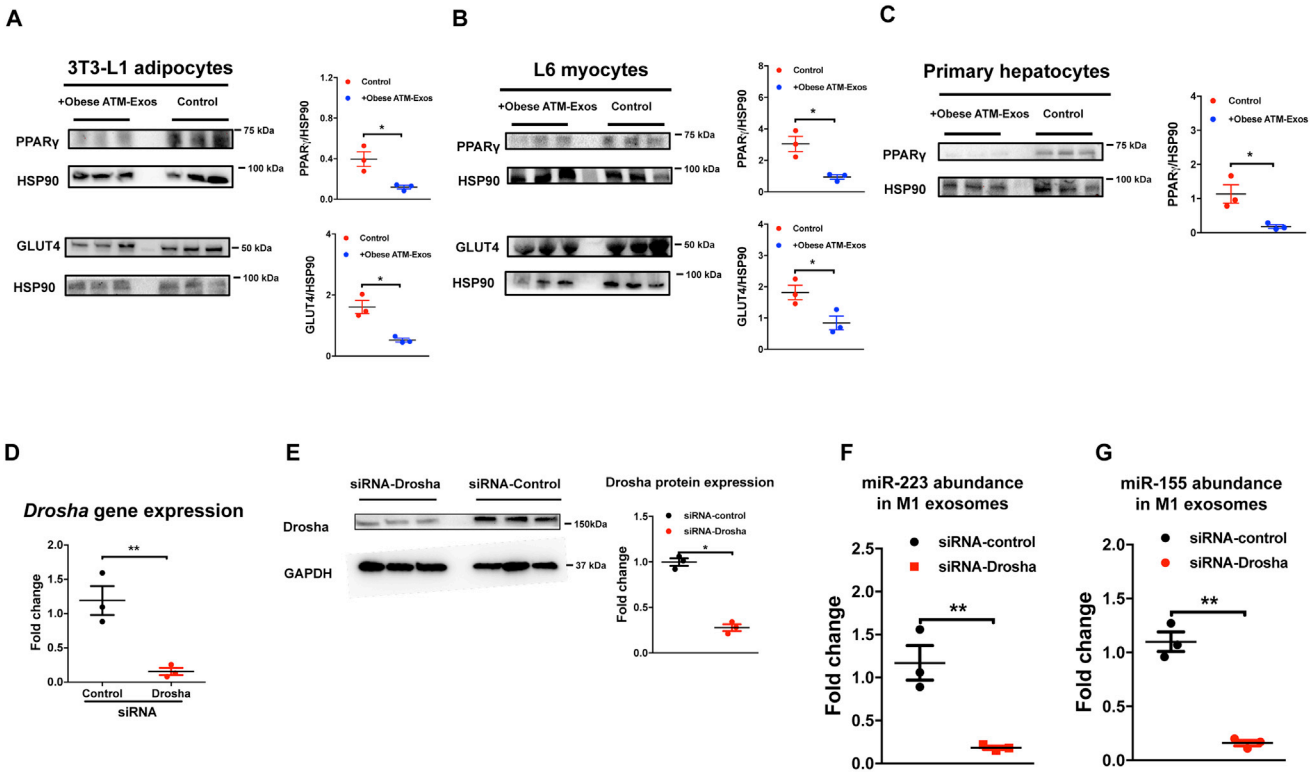


**Figure S3. Effects of Obese ATM-Exos on PPARγ Expression in Insulin Target Cells, Related to Figure 3**

(A–C) Expression of PPARγ in 3T3-L1 adipocytes (A), L6 myocytes (B) and primary hepatocytes (C) after obese ATM exo administration. Levels of the glucose transporter GLUT4 were also measured in adipocytes (A) and myocytes (B). In the western blot analyses, the exposure time to detect PPARγ in 3T3-L1 adipocytes (A), L6 myocytes (B), and primary hepatocytes (C) was 140 s, 460 s, and 480 s, respectively. The exposure time to detect GLUT4 in 3T3-L1 adipocytes and L6 myocytes was 180 s and 100 s, respectively. (D and E) After siRNA-Drosha transfection for 48 hr, the knockdown efficiency of *Drosha* mRNA and protein in M1 macrophages was evaluated by qPCR and western blot analysis. These blots are representative of 3 replicated independent experiments. (F and G) miR-223 and miR-155 abundance in exosomes after knockdown of Drosha. Data are presented as mean ± SEM. (D), (F), and (G) n = 3 per group. *$p < 0.05$, **$p < 0.01$, Student's t test.

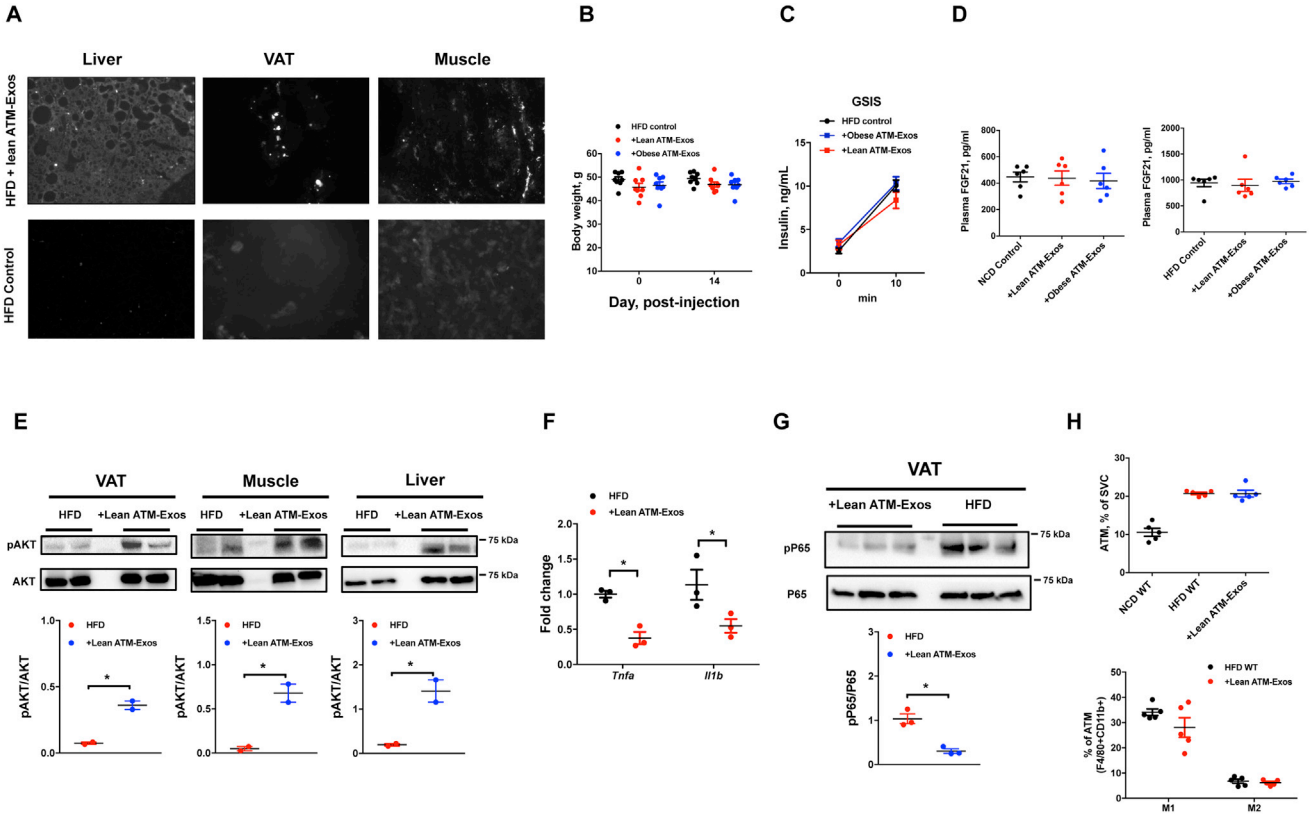


**Figure S4. Effects of Lean ATM-Exos on Metabolism in HFD Recipient Mice, Related to Figure 4**

(A) Appearance of PKH26-labeled Exos in liver, VAT, and muscle of WT HFD recipient mice after 16 hr administration of lean ATM-Exos. Representative images shown from 3 independent experiments. HFD, high-fat diet. (B and C) After treatment with lean ATM-Exos for 2 weeks, body weight (B) and GSIS (C) levels in HFD WT mice treated with ATM-Exos. (D) Circulating FGF21 levels in recipient mice after ATM Exo treatment. (E) Insulin-stimulated AKT phosphorylation in VAT, muscle, and liver of HFD WT recipient mice. These blots are representative of 3 replicated independent experiments. (F and G) Gene expression of proinflammatory cytokines *Tnfa* and *Il1b* (F), and phosphorylation of P65 (G) in VAT of HFD WT mice after ATM exosome treatment. (H) The macrophage population and their phenotypes in VAT of HFD WT recipient mice were examined by flow cytometry analysis. Data are presented as mean ± SEM. (B and C) n = 8 per group; (D) n = 6 per group, (F) n = 4 per group; (H) n = 5 per group. (B) HFD control versus +lean ATM-Exos, p = 0.094 by Student's t test. *p < 0.05. pAKT, phosphorylated AKT. pP65, phosphorylated P65. SVC, stromal vascular cells. ATM, CD11b+F4/80+; M1, CD11b+F4/80+CD11c+CD206-; M2, CD11b+F4/80+CD11c-CD206+.

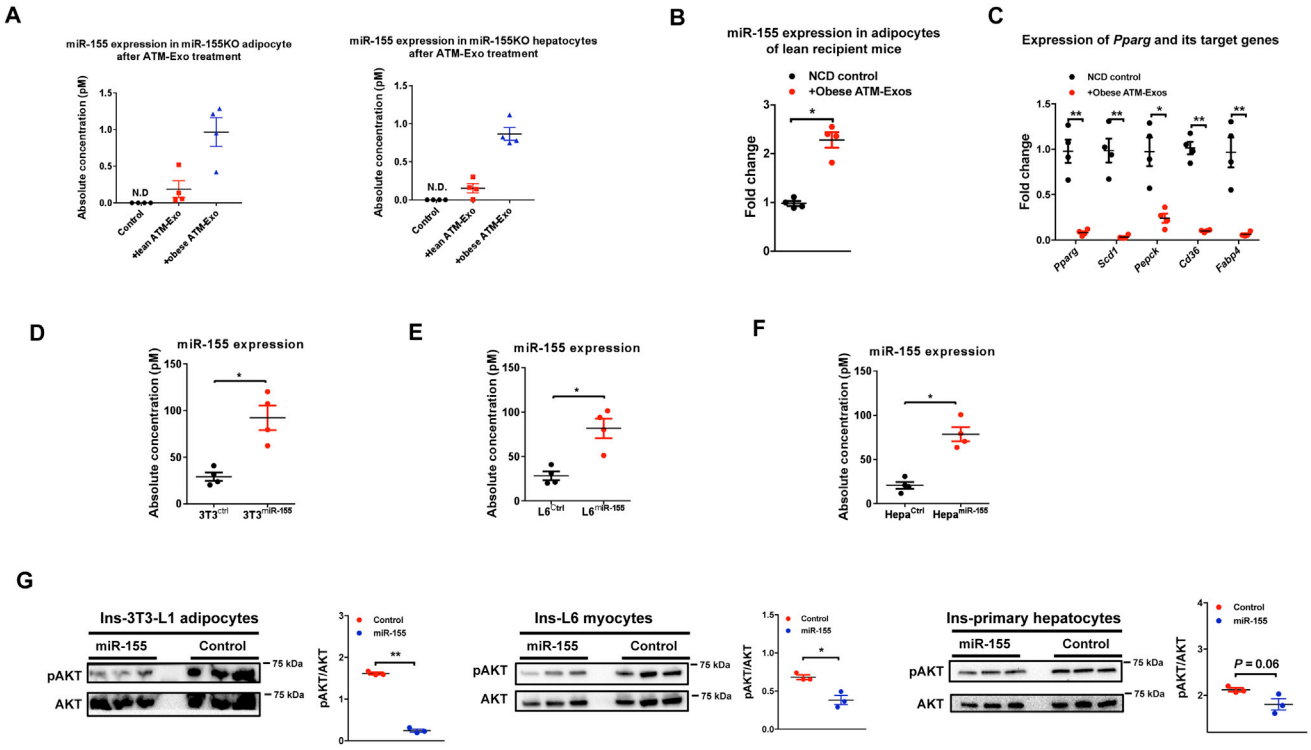


**Figure S5. Effects of miR-155 on PPARγ Expression and Activation of Cellular Insulin Signaling, Related to Figures 5 and 6**

(A) miR-155 expression in the primary miR-155KO adipocytes and hepatocytes after 24 hr ATM-Exo treatment. (B) Abundance of miR-155 in primary adipocytes of NCD WT mice after injection of obese ATM-Exos for 2 weeks. (C) Expression of the miR-155 target gene *Pparg* and related PPARγ target genes in primary adipocytes of NCD WT mice after treatment with obese ATM-Exos. (D–F) The abundance of miR-155 in 3T3-L1 adipocytes (D), L6 myocytes (E), and primary hepatocytes (F) after transfection of miR-155 mimic. The effects of miR-155 on AKT phosphorylation. (G) After overexpression of miR-155, insulin (Ins)-stimulated AKT phosphorylation was measured by western blot analysis. These blots are representative of 3 replicated independent experiments. Data are presented as mean ± SEM. (A–F) n = 4 per group. *$p < 0.05$, **$p < 0.01$, ***$p < 0.001$, Student's t test.

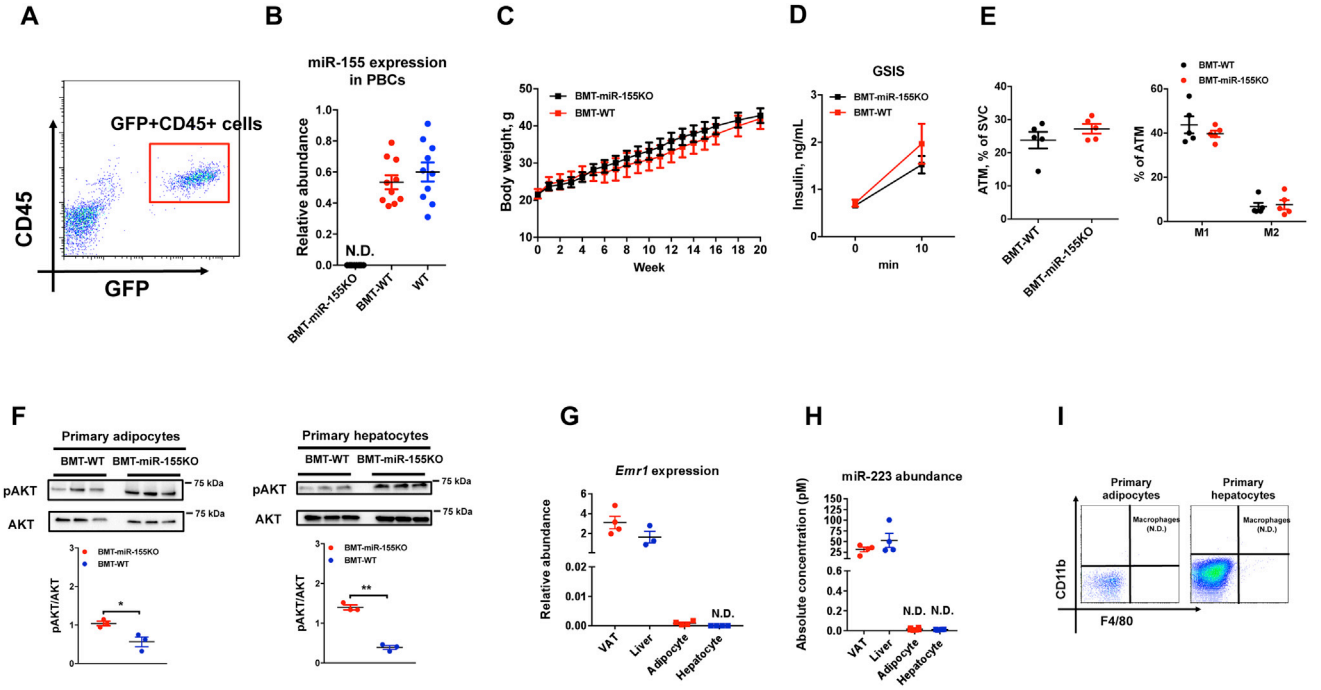


**Figure S6. Effects of ATM-Derived Exosomal miR-155 on Metabolic Phenotypes of miR-155KO Recipient Mice, Related to Figure 7**

(A) Engraftment of donor cells was examined by flow cytometry analysis. (B) miR-155 expression in peripheral blood cells (PBCs) after 20 weeks transplantation of either WT bone marrow (BMT-WT) or miR-155KO bone marrow cells (BMT-miR-155KO). (C) After engraftment was confirmed, mice receiving either bone marrow cells from GFP WT or miR-155KO donor mice were fed HFD and body weight was measured over time. (D) After 20 weeks HFD feeding, GSIS was measured. (E) The macrophage population and their phenotypes in VAT of bone marrow transplanted miR-155KO recipient mice were examined by flow cytometry analysis. (F) Insulin-stimulated AKT phosphorylation in primary adipocytes and hepatocytes of miR-155KO recipient mice after bone marrow transplantation. These blots are representative of 3 replicated independent experiments. (G–I) Macrophages were not present in the isolated primary adipocytes and hepatocytes, as evidenced by non-detectable (N.D.) macrophage-specific genes *Emr1* and miR-223, or cell surface markers (CD11b+F4/80+). Data are presented as mean ± SEM. (B–D) n = 10 per group; (E) n = 5 per group; (G and H) n = 4-6 per group.